



Improvement of inorganic aerosol component in PM_{2.5} by constraining aqueous-phase formation of sulfate in cloud with satellite retrievals: WRF-Chem simulations

Tong Sha^a, Xiaoyan Ma^{a,*}, Jun Wang^b, Rong Tian^a, Jianqi Zhao^a, Fang Cao^c, Yan-Lin Zhang^c

^a Collaborative Innovation Center on Forecast and Evaluation of Meteorological Disasters (CIC-FEMD), Key Laboratory for Aerosol-Cloud-Precipitation of China Meteorological Administration, Nanjing University of Information Science & Technology, Nanjing 210044, China

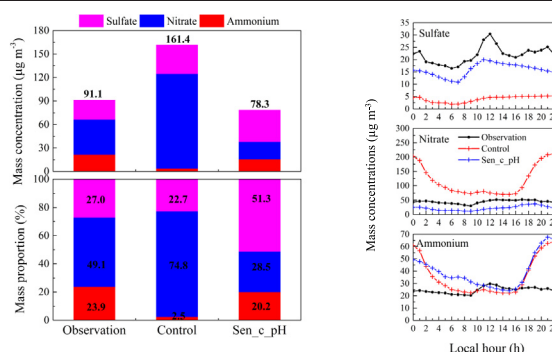
^b Department of Chemical and Biochemical Engineering, Center for Global and Regional Environmental Research, University of Iowa, Iowa City, Iowa 52242, United States

^c Yale-NUIST Center on Atmospheric Environment, International Joint Laboratory on Climate and Environment Change and Key Laboratory Meteorological Disaster, Ministry of Education & Collaborative Innovation Center on Forecast and Evaluation of Meteorological Disaster, Jiangsu Provincial Key Laboratory of Agricultural Meteorology, College of Applied Meteorology, Nanjing University of Information Science and Technology, Nanjing 210044, China

HIGHLIGHTS

- Most numerical models generally underestimate sulfate but overestimate nitrate in PM_{2.5}.
- Uncertainties in cloud water content can contribute to model biases in simulating sulfate, nitrate and ammonium (SNA).
- The model bias in simulating SNA can be reduced by constraining the modelled cloud water with the satellite observations.

GRAPHICAL ABSTRACT



ARTICLE INFO

Article history:

Received 2 July 2021

Received in revised form 18 August 2021

Accepted 5 September 2021

Available online 9 September 2021

Editor: Jianmin Chen

Keywords:

Sulfate
Aqueous-phase chemistry
Cloud water
WRF-Chem
Satellite data

ABSTRACT

High concentrations of PM_{2.5} in China have caused severe visibility degradation and health problems. However, it is still challenging to accurately predict PM_{2.5} and its chemical components in numerical models. In this study, we compared the inorganic aerosol components of PM_{2.5} (sulfate, nitrate, and ammonium (SNA)) simulated by the Weather Research and Forecasting model fully coupled with chemistry (WRF-Chem) model with in-situ data in a heavy haze-fog event during November 2018 in Nanjing, China. Comparisons show that the model underestimates sulfate concentrations by 81% and fails to reproduce the significant increase of sulfate from early morning to noon, which corresponds to the timing of fog dissipation that suggests the model underestimates the aqueous-phase formation of sulfate in clouds. In addition, the model overestimates both nitrate and ammonium concentrations by 184% and 57%, respectively. These overestimates contribute to the simulated SNA being 77.2% higher than observed. However, cloud water content is also underestimated which is a pathway for important aqueous-phase reactions. Therefore, we constrained the simulated cloud water content based on the Moderate Resolution Imaging Spectroradiometer (MODIS) Liquid Water Path observations. Results show that the simulation with MODIS-corrected cloud water content increases the sulfate by a factor of 3, decreases the Normalized Mean Bias (NMB) by 53.5%, and reproduces its diurnal cycle with the peak concentration occurring at noon. The improved sulfate simulation also improves the simulation of nitrate, which decreases the simulated nitrate bias by 134%. Although the simulated ammonium is still higher than the observations, corrected cloud water content leads to a decrease of the modelled bias in SNA from 77.2% to 14.1%. The strong sensitivity of simulated SNA

* Corresponding author.

E-mail address: xma@nuist.edu.cn (X. Ma).

concentration to the cloud water content provides an explanation for the simulated SNA bias. Hence, uncertainties in cloud water content can contribute to model biases in simulating SNA which are less frequently explored from a process-level perspective and can be reduced by constraining the model with satellite observations.

© 2021 Elsevier B.V. All rights reserved.

1. Introduction

Severe and persistent haze pollution with daily concentrations of $\text{PM}_{2.5}$ exceeding the Chinese standard of $75 \mu\text{g m}^{-3}$, occurs frequently in China during recent decades, which has aroused wide public attention due to its adverse impact on air quality, regional and global climate, and human health (Huang et al., 2014). According to previous studies (Liu et al., 2020a; Wu et al., 2019), some of the main factors leading to these haze episodes include, for example, stagnant meteorological conditions with high atmospheric relative humidity and low boundary layer height, high emissions of primary air pollutants, and the rapid formation of secondary inorganic aerosols, consisting of sulfate, nitrate, and ammonium, together named as SNA. Earlier studies showed that the contribution of SNA to total $\text{PM}_{2.5}$ mass concentration was over 50% during severe haze events (Cheng et al., 2016; Wang et al., 2019; Xu et al., 2017).

Chemical transport models (CTMs) are often used to predict $\text{PM}_{2.5}$ pollution and evaluate emission control strategies. Most models show reasonable performance on simulating surface $\text{PM}_{2.5}$ concentrations in China but perform poorly simulating the proportion of chemical components in $\text{PM}_{2.5}$, especially during severe haze periods (Chen et al., 2019; Gao et al., 2018). Many recent studies have concluded that CTMs generally underestimate sulfate concentrations but overestimate nitrate concentrations (Chen et al., 2016; Cheng et al., 2016; Chen et al., 2019; Fu et al., 2016; Gao et al., 2016; Li et al., 2018; Sha et al., 2019a; Wang et al., 2013b; Wang et al., 2014; Zheng et al., 2015a). Uncertainties in meteorological fields (Li et al., 2017c; Su et al., 2018), emission inventories (Ma et al., 2018; Qu et al., 2019; Zhang et al., 2018), and parameterizations of physical and chemical processes in the model (Alexander et al., 2020; Gao et al., 2018; Luo et al., 2019), can contribute to the discrepancies of SNA and $\text{PM}_{2.5}$ between models and observations.

Our previous work indicated that different emission inventories ("bottom-up" and "top-down" SO_2 and NO_x emission estimates) result in a deviation of $4 \mu\text{g m}^{-3}$ and $8 \mu\text{g m}^{-3}$ for the simulated sulfate and nitrate during a haze event in Shanghai, but the simulated sulfate (nitrate) using both inventories are much lower (higher) than the observations (Sha et al., 2019b). Therefore, the incomplete and/or inaccurate chemical mechanism in the model might be another main reason for the underestimation of sulfate and overestimation of nitrate. Generally, sulfate is formed through the gas-phase oxidation of SO_2 by OH radicals, and aqueous-phase oxidation of S(IV) ($= \text{SO}_2 \cdot \text{H}_2\text{O} + \text{HSO}_3^- + \text{SO}_3^{2-}$) by various oxidants (e.g., H_2O_2 , O_3 , NO_2 , and O_2 (transition-metal ion (TMI) catalysis)) in cloud droplets and on the surface of and/or within the bulk preexisting aerosols (the latter multiphase reactions often called heterogeneous reactions) (Liu et al., 2020a; Shao et al., 2019). The nitrate formation includes gas-phase oxidation of NO_x ($\text{NO}_x = \text{NO} + \text{NO}_2$) by OH radicals and O_3 , and hydrolysis of nitrogen pentoxide (N_2O_5) in the preexisting aerosols (Fan et al., 2020a). The aqueous-phase oxidation of NO_x in cloud droplets is much less important than the above two pathways (Jacob, 2000). For ammonium, its formation is mainly from the neutralization/condensation of H_2SO_4 and HNO_3 with NH_3 to form ammonium sulfate ($(\text{NH}_4)_2\text{SO}_4$) or ammonium bisulfate (NH_4HSO_4) and ammonium nitrate (NH_4NO_3), respectively. As H_2SO_4 is nonvolatile, NH_3 prefers to react with H_2SO_4 first especially under warm conditions, while under cooler temperatures, NH_4NO_3 is formed

favorably given sufficient NH_3 although the sulfate is not fully neutralized (Kong et al., 2014). Therefore, the competition between H_2SO_4 and HNO_3 for available NH_3 to form sulfate and ammonium can lead to an underestimation of sulfate in the model that is usually accompanied by an overestimation of nitrate.

In most numerical models, such as the WRF-Chem, the chemical mechanisms of sulfate formation only include the gas-phase and aqueous-phase oxidations of SO_2 , but do not include SO_2 heterogeneous reactions (the main formation mechanisms of sulfate in the standard model are shown in Table S2). Our recent work indicated that tripling the gas-phase oxidation rate of SO_2 by OH in the WRF-Chem model only enhances sulfate by 72% during winter in Nanjing, still 73% lower than the observations, implying gas-phase oxidation is possibly not the major cause for the underestimations in the model (Sha et al., 2019a). Current studies generally believed that the sulfate underestimation might be attributed to the lack of heterogeneous production in the model. The proposed sulfate heterogeneous formation mechanisms include the SO_2 oxidation by NO_2 (Cheng et al., 2016; Wang et al., 2016a), by O_2 via TMI catalysis (Li et al., 2017a) or radical chain reactions (Hung and Hoffmann, 2015; Hung et al., 2018), and by H_2O_2 (Ye et al., 2018). Due to the aerosol water is acidic with the pH value of 3.0–4.9 in China (Ding et al., 2019; Guo et al., 2017), TMI-catalyzed oxidation of SO_2 perhaps dominates the sulfate formation during the haze periods, which is also verified by the observations of sulfate oxygen isotopes (Fan et al., 2020b). However, since the observations of concentration, complexation, and solubility of TMIs, as well as aerosol pH and water content, are not available, the mechanism of sulfate heterogeneous reactions remains unclear (Wang et al., 2020). Therefore, to tackle the underestimation of sulfate, the heterogeneous formation of sulfate was simply parameterized in the model as a reactive uptake process and assuming to be irreversible (Chen et al., 2016; Feng et al., 2018; Li et al., 2017a; Li et al., 2018; Shao et al., 2019; Tian et al., 2021; Wang et al., 2014; Zheng et al., 2015b). Although the implementation of SO_2 heterogeneous reactions in the model achieves an agreement of simulated and observed sulfate concentrations, the model still underestimates sulfate (Huang et al., 2019; Sha et al., 2019a).

In-cloud sulfate formation is known as the major source of global sulfate because aqueous-phase oxidation of S(IV) by H_2O_2 and O_3 occurs much more rapidly than gas-phase oxidation by OH (Barth et al., 2000; Ervens, 2015). Many studies showed that sulfate concentrations are enhanced by the occurrence of cloud and fog compared to cloud-free conditions (Crahan et al., 2004; Ervens et al., 2018; Sorooshian et al., 2006, 2007; Wonaschuetz et al., 2012). Previous modeling studies concluded that a major fraction of sulfate (60–90%) is formed via in-cloud aqueous chemistry globally (Dovrou et al., 2019; Ervens, 2018; Harris et al., 2013; Ma and Salzen, 2006). The rate of in-cloud dissolution and subsequent aqueous-phase reactions of SO_2 depend not only upon chemical parameters such as the availability of oxidants and cloud water pH but also upon cloud microphysical parameters such as the liquid water content (LWC), droplet size distribution and lifetime of cloud droplets (Ervens, 2015). It is noted that the kinetic and mechanistic parameters for the oxidation of S(IV) are relatively well constrained in the model, thus the largest uncertainties in predicting in-cloud sulfate formation originate from the prediction of cloud microphysical parameters (Rasch et al., 2000). Among them, cloud water content is a key parameter to describe the characteristics of cloud fields in the model, which is predicted by the microphysical scheme and then passed to the chemistry module.

Changes in cloud water can affect the dissolved amount of water-soluble atmospheric trace gases such as HNO_3 , HCl , SO_2 , and NH_3 , and thus induces changes in the cloud water pH, which in turn impact the sulfate production (Shah et al., 2020). Therefore, uncertainties in cloud properties due to parameterizations in the model translate into uncertainties in predicting concentrations of sulfate and other chemical species (Barth et al., 2007; Berg et al., 2015; Koch et al., 2003). A previous study found that the simulated sulfate concentrations significantly increase after correcting the underestimation of model cloud fraction (Mueller et al., 2006). Xie et al. (2019) showed that the improvement in cloud fields in Modern Era Retrospective Analysis for Research and Applications, Version 2 (MERRA-2) can eliminate approximately half of the bias in surface sulfate concentrations during summertime relative to the MERRA. However, only a few studies focused on the sulfate underestimation caused by the uncertainties of simulated cloud fields during haze episodes. Therefore, a better understanding of the sensitivity of sulfate formation to cloud water content is needed to improve the model performance on predicting SNA and $\text{PM}_{2.5}$.

A persistent high $\text{PM}_{2.5}$ level accompanying the fog event (short for haze-fog event) occurred in the Yangtze River Delta (YRD) region, China from 26 November to 2 December 2018. We choose this period to investigate the impact of cloud/fog water content on simulating SNA using the WRF-Chem model. The paper is organized as below. Section 2 describes the WRF-Chem model and observation data, as well as presents the meteorology evaluation. The evaluation of simulated chemical fields and cloud water content with observations, and sensitivity experiments to study the impacts of corrected cloud water content on simulated SNA are presented in Section 3. Section 4 is a summary.

2. Model configurations, data description, and model evaluation

2.1. Model configurations

The WRF-Chem model version 3.9.1 (Grell et al., 2005) is used in this study. The model is configured using two nested domains with grid spacings of 27 km and 9 km, respectively. The coarser grids cover eastern China, and the finer grids cover the YRD (Fig. S1). Both domains have 42 vertical levels, with 24 levels below the boundary layer (about 1500 m) and the lowest level about 21 m. Physical schemes include Lin microphysical scheme (Chen and Sun, 2002), Grell 3-D cumulus scheme (Grell and Dezsó, 2002), RRTM (Mlawer et al., 1997) for longwave radiation and Goddard scheme for shortwave radiation (Chou and Suarez, 1994), Yonsei University planetary boundary layer scheme (Hong et al., 2006), QNSE surface layer scheme (Sukoriansky et al., 2005) and Noah land surface model (Tewari et al., 2004). The selection of these configurations is based on our prior sensitivity studies in which this combination yielded the best performance for simulating the haze-fog event in the YRD. The embedded objective analysis programs (OBSGRID) are also used to constrain the ambient meteorology in all experiments, including pressure, air temperature, dew point temperature, wind direction and speed. The U.S. National Center for Environmental Prediction (NCEP) ADP Global Surface Observational Weather Data (<https://rda.ucar.edu/datasets/ds461.0/>) are chosen as the input observation data in OBSGRID to nudge the initial and boundary meteorological conditions and provide surface fields for the surface-analysis-nudging four dimensional data assimilation (FDDA).

The Carbon Bond Mechanism (CBMZ) for gas-phase chemistry (Zaveri and Peters, 1999) and the Model for Simulating Aerosol Interactions and Chemistry (MOSAIC) aerosol module with four sectional aerosol bins and aqueous reactions (Zaveri et al., 2008) are used. MOSAIC predicts all major aerosol species, including sulfate, nitrate, ammonium, BC, primary organic mass, chloride, sodium, other inorganic mass (OIN), and liquid water. The aqueous-phase production is predicted through a bulk cloud water approach (MOSAIC) and subsequently partitioned into the four cloud water bins which connect to the four aerosol size bins. The Fahey and Pandis (2001) aqueous-phase chemistry scheme is

implemented and calculates sulfate formation as well as formaldehyde oxidation and nonreactive uptake of HNO_3 , HCl , NH_3 , and other trace gases. The main aqueous-phase formation mechanisms of sulfate in the current model are summarized in Table S2.

The $0.25^\circ \times 0.25^\circ$ NCEP Final Analysis (FNL) dataset (<http://rda.ucar.edu/datasets/ds083.2/>) provides meteorological initial and boundary conditions. Anthropogenic emissions with a spatial resolution of $0.25^\circ \times 0.25^\circ$ are taken from Multi-resolution Emission Inventory for China (MEIC: <http://www.meicmodel.org/>) for the year 2016 (Li et al., 2017b). The simulation starts on 24 November and ends on 2 December 2018, with the first 48 h used as a spin-up period.

2.2. Observational data

Meteorological variables are measured every three hours from 51 weather stations located in Nanjing and its surrounding cities. These data are obtained from the Meteorological Information Comprehensive Analysis and Process System (MICAPS) (green dots in Fig. 1), which are used to evaluate the model performance on simulating meteorological fields. The data include air temperature, relative humidity at 2 m (T2, RH2), wind speed and direction at 10 m (WS10, WD10), visibility (VIS), and accumulated precipitation (PRE) (the sample frequency of precipitation is 6 hourly).

For evaluating the simulated surface air pollutants, two data sets are used: (1) hourly SO_2 , NH_3 , HNO_3 , HONO, and inorganic chemical components in $\text{PM}_{2.5}$ (sulfate, nitrate, and ammonium) concentrations measured by the In-situ Gas and Aerosol Compositions monitor (IGAC) (Zhan et al., 2021) at Nanjing University of Information Science & Technology (NUIST) (32.2°N , 118.7°E ; 22 m above sea level) (the blue circle in Fig. 1); (2) routinely measurements of hourly SO_2 , NO_2 , and $\text{PM}_{2.5}$ concentrations at 50 monitoring sites from the China National Environmental Monitoring Center (CNEMC), including Nanjing-Maigaoqiao monitoring site (32.1°N , 118.8°E) and 49 sites located in Shanghai, Hangzhou, Hefei, Xuzhou, Heze, Linyi, and Lianyungang (the red circles in Fig. 1). Since the NUIST site did not observe NO_2 and $\text{PM}_{2.5}$ simultaneously, the observed NO_2 and $\text{PM}_{2.5}$ from the Maigaoqiao site close to NUIST are used.

The Advanced Himawari Imager (AHI) data from the Himawari-8 satellite are used to represent the fog area (<https://www.eorc.jaxa.jp/ptree/index.html>). The AHI has 16 channels with central wavelengths ranging from 0.47 μm to 13.3 μm . The spatial resolution of the AHI pixel is 0.5 km for band 3; 1 km for bands 1, 2, and 4; and 2 km for the other bands. Fog area is indicated by the albedo at three visible bands, i.e., red (band 3, 0.64 μm), green (band 2, 0.51 μm), and blue (band 1, 0.47 μm) (Yan et al., 2020). Finally, the daily liquid water path (LWP) observations from Moderate Resolution Imaging Spectroradiometer (MODIS) Aqua Collection 6 Level-3 production with a spatial grid spacing of 1° are used to evaluate the model performance on simulating cloud water content. The confidence quality assessment in MODIS Collection 6 is set to 3 (i.e., high confidence) for all successful retrievals so that quality control is no longer required when we use the dataset (Platnick et al., 2014). Additionally, due to the difference in the spatial resolution between MODIS and simulations, the simulated LWP was oversampled to the MODIS grid cells ($1^\circ \times 1^\circ$) using the nearest neighbor resampling to match the spatial resolution of MODIS LWP.

2.3. Model evaluation

From 26 November to 2 December 2018, the YRD region experienced a severe haze-fog event for seven days (fog areas are shown in Fig. S2). The daily average relative humidity and $\text{PM}_{2.5}$ in many cities exceed 85% and $75 \mu\text{g m}^{-3}$, respectively, and the visibility was less than 50 m in some areas. Such a severe pollution process provides a good opportunity to investigate the aqueous-phase chemistry.

As the large-scale meteorological fields can contribute to the occurrence of fog and clouds which are reactors for aqueous-phase chemistry,

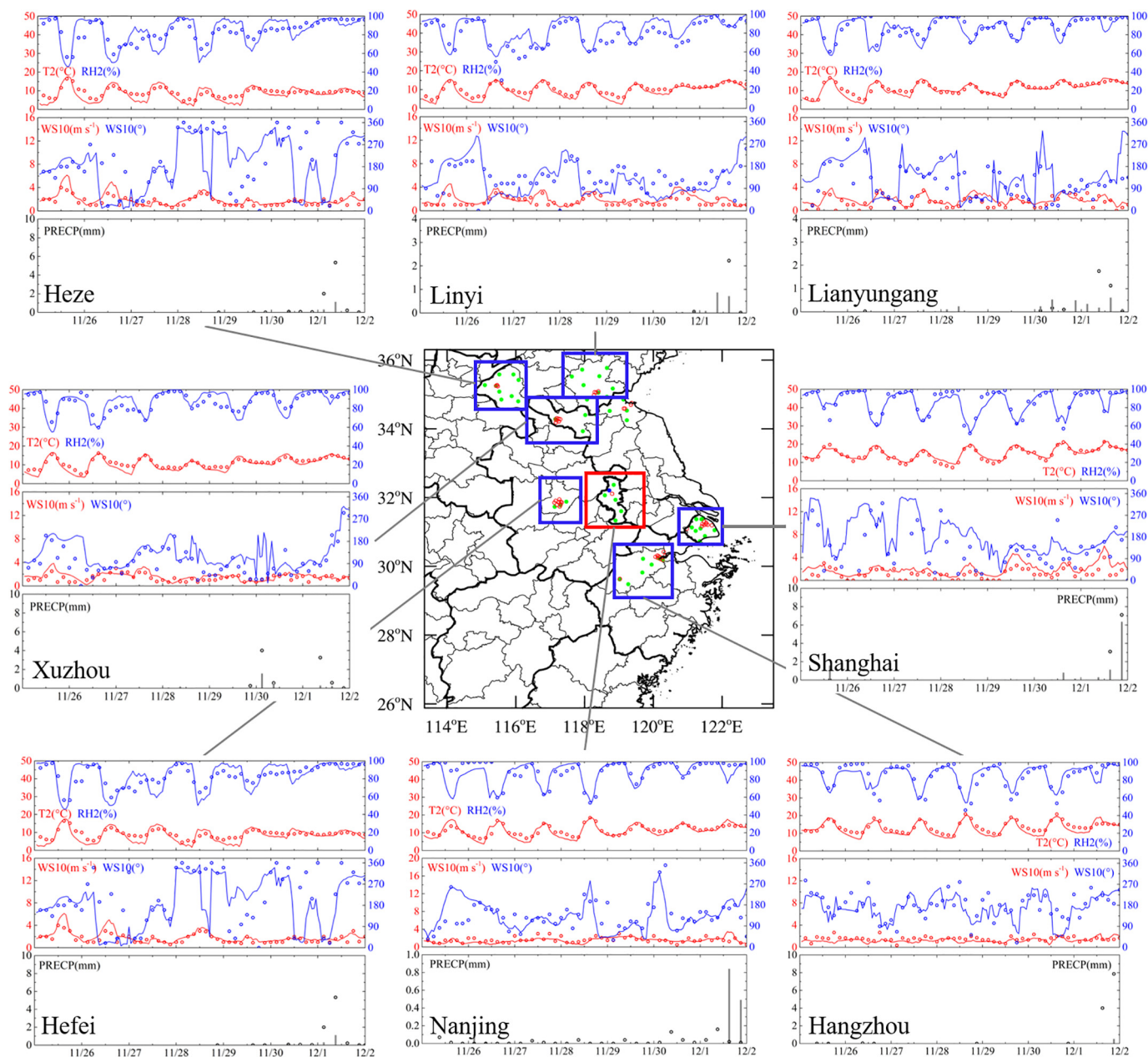


Fig. 1. The performance of simulated hourly meteorological parameters (2 m temperature (T2), 2 m relative humidity (RH2), 10 m wind speed (WS10), 10 m wind direction (WD10), and 6 h accumulation precipitation (PRE)) in 8 typical cities in the YRD, including Nanjing, Hangzhou, Shanghai, Lianyungang, Linyi, Heze, Xuzhou, and Hefei, which all experienced the haze-fog event. Open circles and solid lines (or columns) represent observations and simulations, respectively. The map shows the location of sites with in-situ measurements of meteorological variables and air pollutants (Green dots, red and blue circles denote the routine meteorological stations, air quality monitoring sites, and Nanjing University of Information Science & Technology (NUIST), respectively). (For interpretation of the references to colour in this figure legend, the reader is referred to the web version of this article.)

it is necessary to evaluate the model performance on simulated meteorological parameters over a large region. We compare the simulated meteorology with the observations in 8 typical cities in the YRD, including Nanjing, Hangzhou, Shanghai, Lianyungang, Linyi, Heze, Xuzhou, and Hefei (Fig. 1), which all experienced the haze-fog event. The model can reproduce the temporal variation of observed meteorological variables in all cities, such as T2, RH, WS10, and WD10, with correlation coefficients all larger than 0.85, 0.68, 0.45, and 0.40. The mean biases (MBs) and root-mean-square errors (RMSEs) of hourly T2, RH2, WS10, and WD10 are also small, with the absolute MBs all lower than 1.0 °C, 6.0%, 0.8 m s⁻¹, 36.1° (except WD10 in Shanghai), and RMSEs all lower than 2.2 °C, 10.8%, 1.1 m s⁻¹, 110.7° (Table S3). There was almost no precipitation during this period. Similarly, the simulated

precipitation is also quite limited except on 2 December. Overall, the simulated meteorological fields are reasonable in the YRD.

3. Results and discussions

3.1. Chemical simulations

We compare the spatial distribution of observed and simulated daily SO₂, NO₂, and PM_{2.5} concentrations, the simulated wind speed and direction at 10 m from 26 November to 2 December in the YRD are also shown in Fig. S3. The model can reproduce the characteristics of the spatial distribution of observed air pollutants concentrations over time. The simulated wind speed at 10 m (WS10) is lower than

2 m s^{-1} in the YRD, and such a low wind speed may not be conducive to the advection and diffusion of air pollutants. The easterly wind brings humid air over the ocean to the YRD, resulting in water vapor saturation and high RH. Therefore, high RH promoted the rapid formation of secondary aerosols is the main cause for this large-scale haze-fog event.

Fig. 2 compares the simulated surface routine air pollutants (SO_2 , NO_2 , and $\text{PM}_{2.5}$) concentrations with ground observations in 8 typical cities in the YRD, including Nanjing, Hangzhou, Shanghai, Lianyungang, Linyi, Heze, Xuzhou, and Hefei. We find that the model can reproduce the magnitude of observed daily air pollutants concentrations, and the correlation coefficients for SO_2 , NO_2 , and $\text{PM}_{2.5}$ are 0.3, 0.7, and 0.5, respectively. However, the model overestimates both SO_2 and $\text{PM}_{2.5}$ concentrations by about 80%. One possible reason is that anthropogenic emissions used in this study are for the year 2016 rather than the simulation year, thus resulting in an overestimation of SO_2 and primary particulate mass emissions. Studies showed that the “bottom-up” approach analyzes and integrates air pollutant-related activity data (such as coal power plants, industry, and residential combustion) with emission factors from various agencies and sources to estimate emissions, and it thus has limitations in that it usually has a temporal lag of 2 to 3 years and can quickly become outdated (Wang et al., 2016b). In addition, the low conversion rate of SO_2 to sulfate in the current model is considered to be the main cause for the overestimation of SO_2 (Li et al., 2017a; Sha et al., 2019a; Song et al., 2019). It is worth noting that the simulated SO_2 is higher than the observations in most areas of YRD, while SO_2 concentrations in Lianyungang, a coastal city of YRD, are underestimated. Clean and humid air from the southeast of the ocean prevailed in Lianyungang during this event, thus overestimating wind speed (the simulated and observed wind speed are 1.8 m s^{-1} and 1.5 m s^{-1} , respectively) may lead to the underestimation of SO_2 . The simulated NO_2 bias is much lower

with the Normalized Mean Bias (NMB) of 7%. Overall, the spatial distribution and magnitude of simulated total $\text{PM}_{2.5}$ in the YRD are reasonable. Since the chemical components of aerosols were observed in Nanjing, the following will focus on the impact of cloud water on SNA formation by comparing the differences between the simulated and observed SNA.

According to the observed RH2 and VIS in Nanjing, we divide the haze-fog event into two stages, the formation and development of fog ($\text{RH}_2 \geq 90\%$ and $\text{VIS} \leq 1 \text{ km}$), and the dissipation of fog ($\text{RH}_2 < 90\%$ and $\text{VIS} > 1 \text{ km}$) (Fig. S4) (Liu et al., 2018). The observed sulfate, nitrate, ammonium, and $\text{PM}_{2.5}$ concentrations all increase when fog dissipates, which are 23%, 24%, 14%, and 17% higher than the concentrations in the formation and development of fog. These results are similar to Zou et al. (2020), indicating that the wet deposition effect of fog on aerosol is negligible if the fog cannot form precipitation, and the aerosols can return to the atmosphere from the fog droplets when fog dissipates, i.e., fog facilitates the increase of inorganic aerosol concentrations by aqueous-phase chemistry and plays an important role in the occurrence of haze event in moist areas.

The hourly and diurnal variations of simulated and observed SO_2 , NO_2 , NH_3 , HNO_3 , HONO, SNA, and $\text{PM}_{2.5}$ concentrations in Nanjing are shown in Figs. 3 and 4. The temporal variations of air pollutants from the simulations and observations are generally consistent. However, the model overestimates SO_2 by 114% and underestimates sulfate by over 80%, and thus underestimates the sulfur oxidation ratio (SOR) by 81%. A low oxidation rate of SO_2 to sulfate in the model has been found in previous studies (Gao et al., 2018). Possible explanations are associated with unclear or incomplete chemical mechanisms of sulfate formation in the models (Moch et al., 2018; Shao et al., 2019). Additionally, the observed sulfate concentration has an obvious

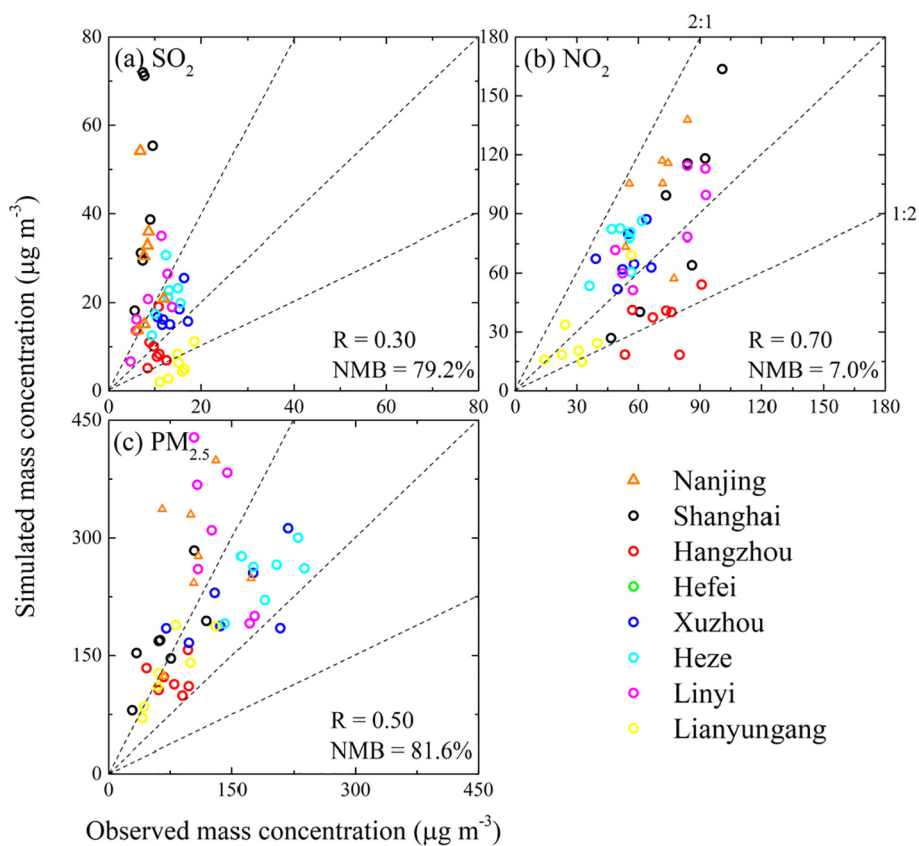


Fig. 2. Scatter plots of daily mean SO_2 , NO_2 , and $\text{PM}_{2.5}$ concentrations from observations (x-axis) versus simulations (y-axis) during the haze-fog event in 8 typical cities in the YRD, including Nanjing, Hangzhou, Shanghai, Lianyungang, Linyi, Heze, Xuzhou, and Hefei, which all experienced the haze-fog event. Also shown on the scatter plots are 1:1, 1:2, and 2:1 line (dash), correlation coefficient (R), and normalized mean bias (NMB).

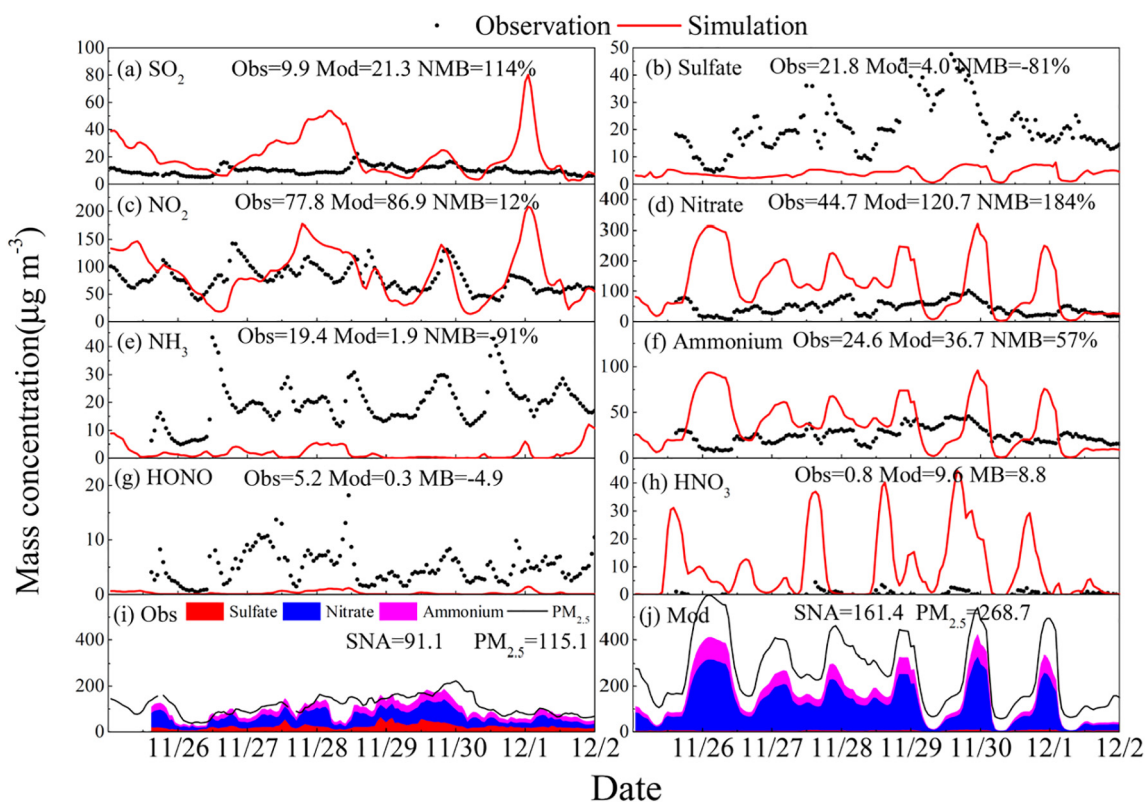


Fig. 3. Time series of the simulated and observed hourly gas precursors concentrations: (a) SO_2 , (c) NO_2 , (e) NH_3 , (g) HONO , (h) HNO_3 , inorganic aerosol concentrations: (b) sulfate, (d) nitrate and (f) ammonium, and the stacked diagram of hourly SNA and $\text{PM}_{2.5}$ concentrations from (i) observations and (j) simulations during the haze-fog event in Nanjing. Statistics in each panel are the mean value of observation (Obs) and model simulation (Mod), mean bias (MB), and normalized mean bias (NMB).

diurnal cycle with the peak occurring at noon, corresponding to the timing of fog dissipation. Sulfate concentrations remain at a relatively high level in fog water during the night and early morning due to the contribution from aqueous-phase chemistry, inducing a significant increase of sulfate when fog droplets evaporate at noon (Xue et al., 2016). However, the simulated sulfate shows a flat diurnal cycle, with a much smaller concentration enhancement rate ($0.45 \mu\text{g m}^{-3} \text{h}^{-1}$) from early morning to noon compared to the observations ($2.3 \mu\text{g m}^{-3} \text{h}^{-1}$), suggesting that model possibly underestimates the formation of sulfate via aqueous-phase chemistry in clouds.

Globally, aqueous sulfate formation is mainly from the oxidation of S(IV) by H_2O_2 and O_3 , and almost 50% from the oxidation by H_2O_2 . Previous studies indicated that the heavy pollution in China is usually associated with weak photochemical activity, impacting photolysis driven atmospheric oxidant species (e.g., OH , H_2O_2 , and O_3), which could suppress the formation of sulfate via the oxidation of S(IV) by H_2O_2 and O_3 during haze-fog events (Li et al., 2017a; Liu et al., 2020b; Wang et al., 2020; Xue et al., 2016). Therefore, the aqueous-phase oxidations of S(IV) by NO_2 and O_2 (TMI-catalyzed) could play an important role in sulfate formation. It is noted that the observed HONO concentrations rise remarkably at noon, which is consistent with the diurnal cycle of sulfate (Fig. 4(b, g)). Additionally, most of the HONO is produced via SO_2 oxidation by NO_2 in the aqueous-phase according to previous studies (Liu et al., 2019). It is therefore suggested that the aqueous-phase oxidation of S(IV) by NO_2 is possibly the main pathway of sulfate formation during this haze-fog event. However, the simulated HONO is almost an order of magnitude lower than the observations and has no obvious diurnal variations as shown in the observations, indicating that the model may underestimate this oxidation pathway of sulfate.

Although the diurnal pattern of NO_2 is consistent in the model and observations, and the averaged NMB is only 12%, the simulated nitrate concentrations are 184% higher than the observations, especially at

night, suggesting that the model overestimates the nitrate nocturnal formation pathway, that is, the N_2O_5 heterogeneous hydrolysis uptake on the surfaces of deliquescence aerosols (Brown et al., 2016; Chang et al., 2016; Lowe et al., 2015). The relatively high N_2O_5 uptake coefficient ($\gamma_{\text{N}_2\text{O}_5}$) and the missing heterogeneous production of nitryl chloride (ClNO_2) from the N_2O_5 uptake on chloride aerosols in the model (the parameterization of $\gamma_{\text{N}_2\text{O}_5}$ is detailed in Supplementary Materials), can both lead to the overestimation of simulated nitrate (McDuffie et al., 2018; Sarwar et al., 2012, 2014). In addition, overestimations of HNO_3 and nitrate (i.e., $\text{TNO}_3 = \text{HNO}_3 + \text{NO}_3^-$) in the model are also attributed to the insufficient removal of TNO_3 (Miao et al., 2020). Therefore, too much TNO_3 may consume a large amount of NH_3 to a certain extent, further inhibiting sulfate formation.

The molar concentrations of total ammonium ($\text{TNH}_4 = \text{NH}_3 + \text{NH}_4^+$) are generally consistent in the simulations (2.1 mol m^{-3}) and observations (2.5 mol m^{-3}), but the simulated NH_3 is 91% lower and ammonium is 57% higher than the observations (Fig. 3(e, f)). This is partly due to the overestimation of TNO_3 in the model (Wang et al., 2013b). On the other hand, aerosol acidity is a key factor driving the semi-volatile partitioning of aerosol species, and lower aerosol water pH is conducive to ammonium in the particle phase. We compare the simulated and observed $\text{PM}_{2.5}$ pH calculated offline using the same thermodynamic model, ISORROPIA II (Fountoukis and Nenes, 2007). The calculation of $\text{PM}_{2.5}$ pH is dependent on the concentrations of aerosol components (i.e., Na^+ , SO_4^{2-} , NH_4^+ , NO_3^- , Cl^- , Ca^{2+} , K^+ , Mg^{2+}) and meteorological variables (i.e., RH and temperature). As shown in Fig. S5, the model underestimates $\text{PM}_{2.5}$ pH by 0.8, contributing to the discrepancies of TNH_4 gas-particle partitioning.

The simulated $\text{PM}_{2.5}$ concentrations are significantly higher than the observations by a factor of 1.3. As CBMZ-MOSAIC only predicts primary organic species but does not consider the formation of secondary organic aerosol, the organic mass concentration must assumedly be underestimated in the model. Therefore, the overestimation of $\text{PM}_{2.5}$

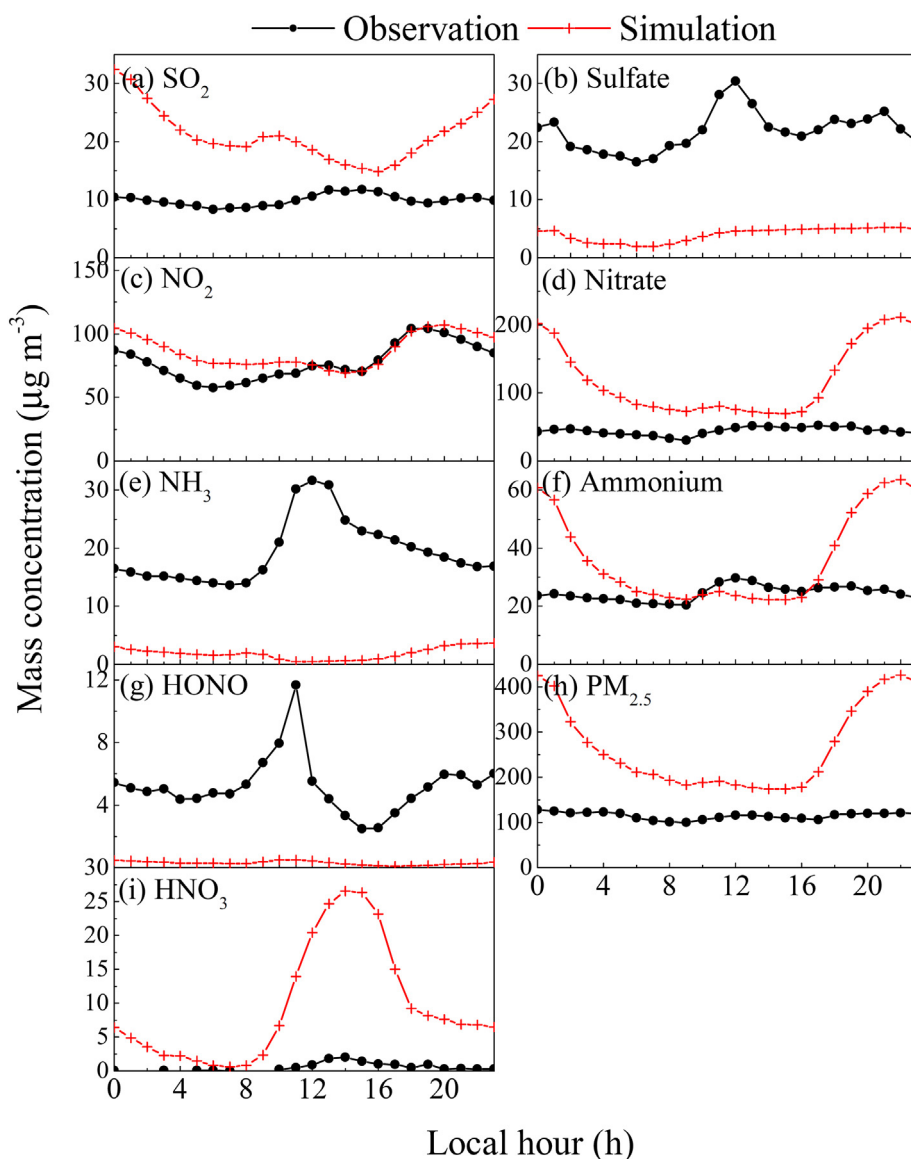


Fig. 4. Diurnal cycles of the simulated and observed mass concentrations of gas precursors: (a) SO_2 , (c) NO_2 , (e) NH_3 , (g) HONO , (i) HNO_3 , and inorganic aerosol concentrations: (b) sulfate, (d) nitrate, (f) ammonium and (h) $\text{PM}_{2.5}$, averaged during the haze-fog event in Nanjing.

is mainly due to the overestimation of SNA, namely nitrate and ammonium. Additionally, the overestimation of primary inorganic aerosols concentrations in the model can also lead to a positive bias of $\text{PM}_{2.5}$.

3.2. Cloud water content

Based on the above analysis, we speculate that the underestimation of sulfate in the model is due to the insufficient in-cloud aqueous-phase formation and/or missing mechanisms in the model. The cloud water is the most uncertain factor to modulate in-cloud aqueous-phase chemistry (Ervens, 2015; Xie et al., 2019). Therefore, it is necessary to evaluate the simulated cloud water content in the model.

The spatial distribution of simulated LWP from 26 November to 2 December in the YRD is shown in Fig. S6. Any model grids with LWP larger than 0.01 g kg^{-1} are defined as fog pixels (Zhou and Du, 2010), and below 1500 m are integrated to calculate the simulated LWP, and LWP larger than 2 g m^{-2} is identified as the fog area (Jia et al., 2019). The model can generally reproduce the distribution characteristics of the fog area observed at 08:00 every day during this period, except on 27 November (the observed fog areas are shown in Fig. S2).

The LWC at the lowest level in the model has an important impact on the SNA formation at the surface. LWC was not observed simultaneously during this period, so visibility (VIS) is usually used to assess the simulated LWC as it is a function of LWC and cloud droplet number (N_c) (Eq. (1); Gultepe et al., 2006).

$$\text{VIS}[\text{m}] = 1002 / (\text{LWC}[\text{g cm}^{-3}] \times N_c[\text{cm}^{-3}])^{0.6473} \quad (1)$$

We compare the spatial distribution of VIS from simulations and observations (threshold of VIS < 1000 m) (Fig. S7), and find that the simulated VIS has a similar spatial pattern with the observed VIS. Although the visibility is underestimated in some areas, the statistics of average visibility over the region where the fog occurred show that the model generally overestimates VIS during the haze-fog event, except on 26 and 29 November. This overestimation is likely caused by the underestimation of LWC in the model. The underestimation of LWC during this period may also be related to the bulk microphysical scheme used in the model (Jia et al., 2019; Khain et al., 2009).

To quantitatively evaluate the modelled cloud water content, we compare the simulated LWP with the MODIS observations. The model

can reproduce the spatial distribution of observed LWP but underestimates LWP in some areas, e.g., Jiangsu Province (Fig. S8). Comparisons of the cumulative probability distribution of the simulated and observed LWP are shown in Fig. 5. The probability distribution of simulated LWP is mainly concentrated in lower LWP, e.g., the probability of simulated LWP less than 20 g m^{-2} is $\sim 80\%$, while the observed one is only 30% (Table S4). The modelled probabilities are 49% lower than the observed ones for larger LWP ($>20 \text{ g m}^{-2}$). The underestimation of LWP in the model is consistent with previous studies (Kay et al., 2012; Mueller et al., 2006; Sha et al., 2019a; Wang et al., 2013a).

As stated above, the model underestimates the sulfate concentrations and cloud water content simultaneously during the haze-fog event. The underestimation of cloud water content possibly leads to the insufficient contribution of in-cloud aqueous-phase chemistry to sulfate formation, which could explain the underestimation of sulfate during the haze episode, but has been overlooked by most previous studies. Therefore, in the next section we use the observed LWP from MODIS to constrain the simulations and explore the impact of cloud water on SNA simulations.

3.3. Sensitivity experiments

3.3.1. Constraining cloud water content in the model

A logarithmic function is used to fit the cumulative density function (CDF) for both observed and simulated LWP values (Fig. 5). The fitting equations are:

$$F_o = -6.4 + 16.5 \ln(x + 1.0) \quad (0 \leq x \leq 500 \text{ g m}^{-2}) \quad (2)$$

$$F_m = 59.1 + 6.7 \ln(x + 5.8) \quad (0 \leq x \leq 500 \text{ g m}^{-2}) \quad (3)$$

where subscripts o and m represent the observation and model, and F and x represent the CDF and LWP, respectively. To update the modelled LWP with satellite observations, we use the histogram matching method (Richards, 2013), so that the CDF function of the simulated LWP after constraining is the same as the observations, i.e., $F_m^c = F_o$. Consequently, the equation for transforming the modelled LWP is:

$$x^c = \begin{cases} 0 & (x = 0 \text{ g m}^{-2}) \\ 53.0 \times (x + 5.8)^{0.4} - 1 & (0 < x \leq 500 \text{ g m}^{-2}) \end{cases} \quad (4)$$

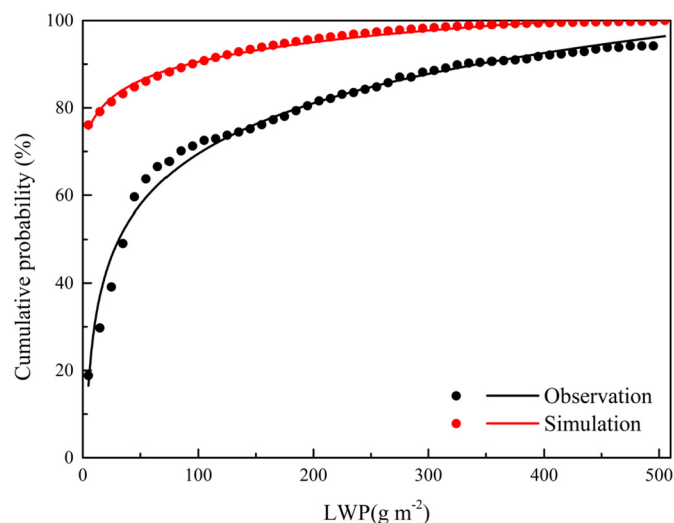


Fig. 5. The cumulative probability distribution of LWP between the MODIS observations and simulations shown as circles. Results are based on statistics of the observed and simulated daily LWP during the haze-fog event over YRD. The lines are the fitting functions.

where c represents the correction with MODIS observations. Note that for the grid with the observed LWP is equal to 0 g m^{-2} , that is, there is no fog occurred, then the modelled LWP is corrected to 0 g m^{-2} .

We apply Eq. (4) to modify the cloud water content in the aqueous-phase chemistry module only and keep the cloud water amount in other modules (i.e., microphysics, cumulus parameterization, dry deposition, wet scavenging, photolysis rates, and radiative transfer modules) unchanged to ensure that other physical and chemical processes are self-consistent between the control and sensitivity model simulations. This is the first sensitivity experiment we conducted, denoted as Sen_c. Consequently, the changes do not affect the cloud properties used in the radiative transfer calculations, and dry/wet deposition, etc. However, cloud-induced changes in aqueous-phase production do alter the mixing ratios of SO_2 and other oxidants (e.g., OH and H_2O_2), which could in turn affect the rate of gas phase oxidation. In addition, the increase of cloud water content can draw more water-soluble atmospheric trace gases such as HNO_3 , HCl, SO_2 , and NH_3 into the solution. Compared to SO_2 , HNO_3 is one of major strong acids in the atmosphere and thus could dissociate completely in cloud water (Table S5), which in turn increase the cloud water acidity when atmospheric ammonia is not sufficient to neutralize hydrogen ions (H^+) in the solution (Shah et al., 2020). This indicates that the amount of HNO_3 dissolved in cloud water may mainly determine the changes in cloud water pH. From Fig. S9, we find that the aqueous-phase fraction of NO_3^- (calculated as the ratio of aqueous-phase concentrations of NO_3^- in clouds and the overall multiphase concentrations, i.e., the sum of in gas and aqueous phase, including undissociated and dissociated forms of NO_3^-) increases with LWP and is correlated with lower cloud water pH in both Control run and Sen_c sensitivity experiment. Therefore, constraining the simulated cloud water content alone results in a decrease in cloud water pH (4.9 to 2.5) during this period (Fig. S9). According to previous studies, the observed cloud water pH in Nanjing during late autumn and winter ranges from 4.3 to 7.6 (Table S6), thus the cloud water pH in the model may be underestimated. To make the cloud water pH in the sensitivity experiment be the same as that of the Control run and as close as possible to the observed pH value, we increase the cloud water pH by 2 units, i.e., decrease the concentrations of hydrogen ion (i.e., $[\text{H}^+]$) by a factor of 100 in another sensitivity experiment (Sen_c_pH). The descriptions of all the experiments are summarized in Table 1.

3.3.2. Impact of cloud constraint on SNA

The differences in the spatial distribution of simulated SNA by the two experiments (Control and Sen_c_pH) are shown in Fig. S11. We find that the simulated sulfate concentration in Sen_c_pH is $6 \mu\text{g m}^{-3}$ larger than the Control over the entire YRD, with the biggest difference in the south of Jiangsu and the east of Anhui province, corresponding to the area most affected by this haze-fog event. The corrected cloud water content increases the contribution of aqueous-phase chemistry to the sulfate formation, thereby reducing the negative bias of simulated sulfate. The formation of sulfate greatly limits the nitrate production, so the simulated nitrate in Sen_c_pH is decreased by $35 \mu\text{g m}^{-3}$ compared to the Control over the entire YRD. However, the ammonium simulated by Sen_c_pH is larger than the results of Control run in most areas of

Table 1
Descriptions of the model simulations.

Experiment name	Description
Control	Control simulation.
Sen_c	Only constrain the simulated LWP according to Eq. (4) in the aqueous-phase chemistry.
Sen_c_pH	Constrain the simulated LWP according to Eq. (4) in the aqueous-phase chemistry and increase the cloud water pH by 2 units.

YRD, with the average difference of $9 \mu\text{g m}^{-3}$. As the inorganic aerosol system is essentially an acid-base titration, an increase in S(VI) concentration can neutralize more NH_3 to form ammonium sulfate ($(\text{NH}_4)_2\text{SO}_4$) or ammonium bisulfate (NH_4HSO_4), leading to an increase of simulated ammonium concentrations.

As shown in Fig. 6, the Sen_c_pH significantly improves the simulation of sulfate in Nanjing. It increases the sulfate concentration by $11.8 \mu\text{g m}^{-3}$ (295%) and decreases the NMB by 53.5%. Also, the Sen_c_pH simulation using corrected cloud water content can reproduce the diurnal cycle and capture the peak concentration of sulfate at noon, with the concentration increasing at a rate of $1.8 \mu\text{g m}^{-3} \text{h}^{-1}$ from early morning to noon, which is not seen in the Control run. Additionally, the Sen_c_pH improves the simulated gaseous SO_2 and O_3 , and the NMB of SO_2 and O_3 decreases by 20% and 48%, respectively, indicating that both sulfate and gaseous SO_2 and O_3 can be better reproduced by improving cloud water content in the model (Fig. S12). Meanwhile, the Sen_c_pH decreases the absolute bias of simulated nitrate from 184.0% to 50.1% compared with the Control run. It greatly reduces the nitrate concentration at night and thus predicts a better diurnal cycle. However, the Sen_c_pH simulation leads to a minor increase in the ammonium concentration. The underestimation of nitrate and overestimation of ammonium in Sen_c_pH could be ascribed to the underestimation of aerosol water pH in the model. The hydrogen ion activity in aerosol water can affect the partitioning of TNO_3 and TNH_4 between the gas and aerosol phase. Lower aerosol water pH favors partitioning of TNO_3 toward gaseous HNO_3 rather than the aerosol nitrate. In contrast, TNH_4 partitions toward gaseous NH_3 at higher aerosol water pH (Weber et al., 2016). The simulated

$\text{PM}_{2.5}$ pH in Sen_c_pH is lower than the observations (Fig. S5), which is conducive to the existence of HNO_3 and aerosol ammonium.

Overall, the simulation with MODIS-corrected cloud water content can decrease the model bias of SNA from 77.2% (Control) to 14.1% (Sen_c_pH) (Fig. 7(a)). The proportion of sulfate in SNA also significantly increases from 2.5% (Control) to 20.2% (Sen_c_pH), which is closer to the observation (23.9%) (Fig. 7(b)), but the Sen_c_pH still underestimates the sulfate concentration by $6 \mu\text{g m}^{-3}$ compared to the observations. A few possibilities can explain the discrepancies. The model possibly underestimates the cloud water pH, with a value of 3.3 in Sen_c_pH (Fig. S13), which is lower than the global typical cloud/fog water pH of 3–6 and the mean value of 4–6 suggested by Pye et al. (2020). The observed fog water pH in Nanjing from previous studies (Hong et al., 2019; Li et al., 2008; Lu et al., 2010; Qin et al., 2011; Yan et al., 2013; Yang et al., 2009; Zhu et al., 2020) are summarized in Table S6, suggesting that the fog water pH during late autumn and winter in Nanjing is generally between 4.3 and 7.6. Therefore, the lower fog water pH simulated by the model could limit the aqueous-phase formation of sulfate to some extent. Note that the aqueous-phase oxidation of S(IV) by NO_2 requires a cloud water pH of about 6, thus the more acidic cloud water in the model is not conducive to this reaction. Consequently, the simulated NO_2 concentrations in Sen_c_pH only change slightly (Fig. S12). Moreover, the model lacks SO_2 heterogeneous reactions on the surface of and/or within the bulk preexisting aerosols (Li et al., 2017a; Shao et al., 2019) and other aqueous-phase reactions in clouds, such as the aqueous oxidation of S(IV) by HCHO and hydroxyl hydroperoxide (ISOPHOH) to form hydroxy-methane sulfonate (HMS) and sulfate (Dovrou et al., 2019;

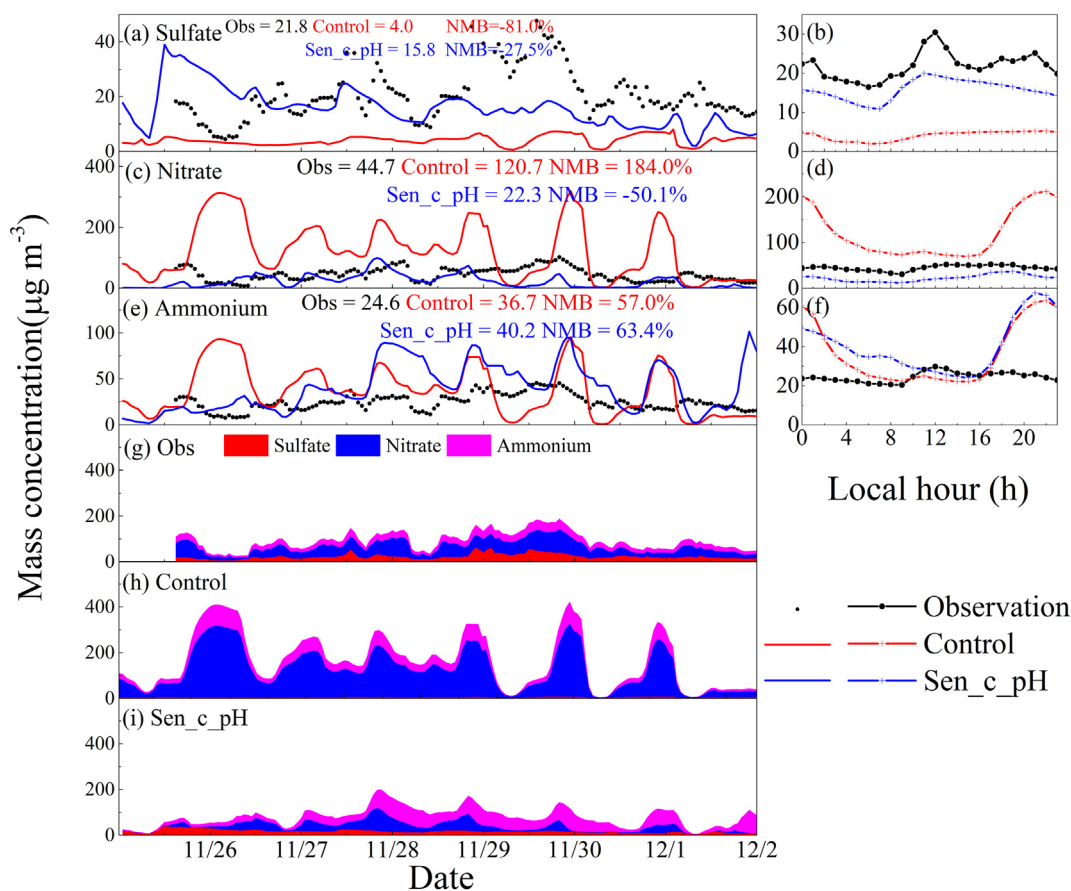


Fig. 6. The hourly and diurnal variations of simulated (Control and Sen_c_pH) and observed (a, b) sulfate, (c, d) nitrate, and (e, f) ammonium concentrations. The stacked diagram of hourly SNA concentrations from (g) observations, (h) Control run, and (i) Sen_c_pH simulations during the haze-fog event in Nanjing. Statistics in panel (a, c, e) are the mean value of observation (Obs) and model simulation (Mod), and NMB.

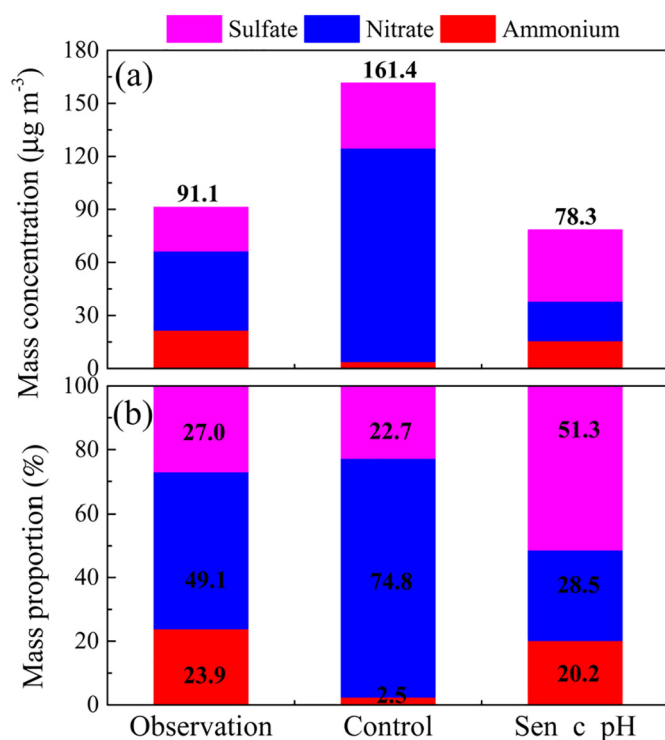


Fig. 7. (a) The average mass concentrations and (b) proportion of the observed and simulated (Control and Sen_c_pH) SNA during the haze-fog event in Nanjing.

Moch et al., 2018), which could also explain the sulfate underestimation even though the cloud water content has already been corrected. In addition, field measurements of aerosols use the method of ion chromatography, such as the IGAC sampling instrument, which easily misinterpret organosulfur (mainly in the presence of HMS) as inorganic sulfate. Moch et al. (2020) suggested that HMS accounts for 25% or more of particulate sulfate in polluted regions of China, which is relatively high on cloudy days. Aerosol mass spectrometry (AMS) measurements in Beijing also showed the presence of HMS up to 30% of particulate sulfur concentrations during winter haze events (Song et al., 2019). Therefore, the presence of HMS can lead to a positive deviation in observed inorganic sulfate. Cloud constraints are based on the MODIS LWP, which has a reported uncertainty range of $\pm 30\%$ (Dong et al., 2008; Khanal and Wang, 2018; Min et al., 2012).

4. Conclusions

In this study, we evaluated the WRF-Chem performance on simulating inorganic aerosol components of PM_{2.5} during a haze-fog event in Nanjing, China, and investigated the model bias caused by the uncertainties of in-cloud aqueous-phase chemistry on simulating SNA.

Our results show that WRF-Chem simulations overestimate SO₂ concentration by 114%, underestimate sulfate concentration by 81%, and fail to reproduce the diurnal cycle of sulfate, which peaks at noon, corresponding to the timing of fog dissipation. In contrast, the model bias of NO₂ is much smaller (NMB = 12%), but the nitrate concentration is overestimated by 184%, especially its nocturnal concentration. Although the molar concentrations of total ammonium are generally consistent between the simulations and observations, the model underestimates NH₃ concentration by 91% and overestimates ammonium concentration by 57%.

Aqueous-phase formation is an important pathway in which dissolved SO₂ in cloud/fog droplets reacts with oxidants to form sulfate. The underestimated cloud water content in the model is constrained by using the MODIS LWP, and sensitivity experiments are also conducted to explore the impact of corrected cloud water content on SNA

simulation. Compared with the Control run, the simulation with MODIS-corrected cloud water content significantly improves the simulation of sulfate by increasing the concentration nearly 3 times, decreases NMB by 53.5%, and reproduces the diurnal peak. Improved sulfate treatment improves the nitrate simulations by altering the sensitivity of nitrate formation to HNO₃ and NH₃, thus the simulated nitrate bias is decreased by 134%, and diurnal cycle representation is also improved. Although the simulated ammonium is higher than the Control run and observation, correcting the cloud water decreases the overall model bias of SNA from 77.2% (Control) to 14.1%.

However, even after the MODIS-based adjustment of cloud water content, the simulated sulfate is still 27.5% lower than the observations. It is found that the model possibly underestimates the cloud water pH (value of 3.3), which is not conducive to the in-cloud aqueous-phase oxidation of S(IV) by NO₂. Missing SO₂ heterogeneous reactions on aerosol water (e.g., TMI-catalyzed oxidation) and other in-cloud aqueous-phase reactions (e.g., S(IV) oxidation by HCHO and ISOPHOH) in the model can also contribute to underestimating the sulfate concentration. In addition, the aerosol measurements and MODIS observations themselves are subject to uncertainties.

Our results emphasize the critical role of cloud water content in simulating SNA, and provide a new perspective on the causes of sulfate underestimation discussed by previous studies. Therefore, we recommend that chemical transport models need to better represent the temporal and spatial distribution of modelled cloud fields to improve haze prediction in the future. This can be achieved by using data assimilation to constrain the ambient meteorology, directly assimilating cloud-related satellite observations into the model, and optimizing the microphysical scheme in the model.

CRediT authorship contribution statement

Tong Sha: Conceptualization, Methodology, Software, Formal analysis, Writing – original draft. **Xiaoyan Ma:** Conceptualization, Writing – review & editing, Supervision. **Jun Wang:** Methodology, Writing – review & editing, Supervision. **Rong Tian:** Writing – review & editing. **Jianqi Zhao:** Writing – review & editing. **Fang Cao:** Data curation. **Yan-Lin Zhang:** Data curation.

Declaration of competing interest

The authors declare that they have no known competing financial interests or personal relationships that could have appeared to influence the work reported in this paper.

Acknowledgments

This study is supported by the National Natural Science Foundation of China grants (41975002 & 42061134009), the Second Tibetan Plateau Scientific Expedition and Research (STEP) program (2019QZKK0103), and the National Key Research and Development Program of China grant (2019YFA0606802). Jun Wang's participation in this project is made possible through in-kind support from the University of Iowa.

Appendix A. Supplementary data

Supplementary data to this article can be found online at <https://doi.org/10.1016/j.scitotenv.2021.150229>.

References

- Alexander, B., Sherwen, T., Holmes, C.D., Fisher, J.A., Chen, Q., Evans, M.J., Kasibhatla, P., 2020. Global inorganic nitrate production mechanisms: comparison of a global model with nitrate isotope observations. *Atmos. Chem. Phys.* 20, 3859–3877. <https://doi.org/10.5194/acp-20-3859-2020>.
- Barth, M.C., Kim, S.-W., Wang, C., Pickering, K.E., Ott, L.E., Stenchikov, G., Leriche, M., Cautenet, S., Pinty, J.-P., Barthe, Ch., Mari, C., Helsdon, J.H., Farley, R.D., Fridlind,

- A.M., Ackerman, A.S., Spiridonov, V., Telenta, B., 2007. Cloud-scale model intercomparison of chemical constituent transport in deep convection. *Atmos. Chem. Phys.* 7, 4709–4731. <https://doi.org/10.5194/acp-7-4709-2007>.
- Barth, M.C., Rasch, P.J., Kiehl, J.T., Benkovitz, C.M., Schwartz, S.E., 2000. Sulfur chemistry in the national center for atmospheric research community climate model: description, evaluation, features and sensitivity to aqueous chemistry. *J. Geophys. Res. Atmos.* 105, 1387–1415.
- Berg, L.K., Shrivastava, M., Easter, R.C., Fast, J.D., Chapman, E.G., Liu, Y., Ferrare, R.A., 2015. A new WRF-chem treatment for studying regional-scale impacts of cloud processes on aerosol and trace gases in parameterized cumuli. *Geosci. Model Dev.* 8 (2), 409–429. <https://doi.org/10.5194/gmd-8-409-2015>.
- Brown, S.S., Dubé, W.P., Tham, Y.J., Zha, Q., Xue, L., Poon, S., Wang, Z., Blake, D.R., Tsui, W., Parrish, D.D., Wang, T., 2016. Nighttime chemistry at a high altitude site above Hong Kong. *J. Geophys. Res.* 121, 2457–2475. <https://doi.org/10.1002/2015JD024566>.
- Chang, W.L., Brown, S.S., Stutz, J., Middlebrook, A.M., Bahreini, R., Wagner, N.L., Dubé, W.P., Pollack, I.B., Ryerson, T.B., Riener, N., 2016. Evaluating N2O5 heterogeneous hydrolysis parameterizations for CalNex 2010. *J. Geophys. Res.* 121, 5051–5070. <https://doi.org/10.1002/2015JD024737>.
- Chen, D., Liu, Z.Q., Fast, J., Ban, J.M., 2016. Simulations of sulfate–nitrate–ammonium (SNA) aerosols during the extreme haze events over northern China in October 2014. *Atmos. Chem. Phys.* 16 (16), 10707–10724.
- Chen, L., Gao, Y., Zhang, M., Fu, J.S., Zhu, J., Liao, H., Li, J., Huang, K., Ge, B., Wang, X., Lam, Y.F., Lin, C.Y., Itahashi, S., Nagashima, T., Kajino, M., Yamaji, K., Wang, Z., Kurokawa, J., 2019. MICS-Asia III: multi-model comparison and evaluation of aerosol over East Asia. *Atmos. Chem. Phys.* 19, 11911–11937. <https://doi.org/10.5194/acp-19-11911-2019>.
- Chen, S.H., Sun, W.Y., 2002. A one-dimensional time dependent cloud model. *J. Meteor. Soc. Japan* 80 (1), 99–118. <https://doi.org/10.2151/jmsj.80.99>.
- Cheng, Y.F., Zheng, G.J., Wei, C., Mu, Q., Zheng, B., Wang, Z.B., Gao, M., Zhang, Q., He, K.B., Gregory, R.C., Ulrich, P., Su, H., 2016. Reactive nitrogen chemistry in aerosol water as a source of sulfate during haze events in China. *Sci. Adv.* 2 (12), 1601530.
- Chou, M.D., Suarez, M.J., 1994. An efficient thermal infrared radiation parameterization for use in general circulation models. *NASA Tech. Memo* 104606 (3) 85pp.
- Crahan, K.K., Hegg, D., Covert, D.S., Jonsson, H., 2004. An exploration of aqueous oxalic acid production in the coastal marine atmosphere. *Atmos. Environ.* 38, 3757–3764. <https://doi.org/10.1016/j.atmosenv.2004.04.009>.
- Ding, J., Zhao, P., Su, J., Dong, Q., Du, X., Zhang, Y., 2019. Aerosol pH and its driving factors in Beijing. *Atmos. Chem. Phys.* 19, 7939–7954. <https://doi.org/10.5194/acp-19-7939-2019>.
- Dong, X.Q., Minnis, P., Xi, B., Sun-Mack, S., Chen, Y., 2008. Comparison of CERES-MODIS stratus cloud properties with ground-based measurements at the DOE ARM southern Great Plains site. *J. Geophys. Res. Atmos.* 113, D03204. <https://doi.org/10.1029/2007JD008438>.
- Dovrou, E., Rivera-Rios, J.C., Bates, K.H., Keutsch, F.N., 2019. Sulfate formation via cloud processing from isoprene hydroxyl hydroperoxides (ISOPPOH). *Environ. Sci. Technol.* 53, 12476–12484.
- Ervens, B., 2015. Modeling the processing of aerosol and trace gases in clouds and fogs. *Chem. Rev.* 115 (10), 4157–4198.
- Ervens, B., 2018. Progress and problems in modeling chemical processing in cloud droplets and wet aerosol particles. *ACS Symp. Ser.* 1299, 327–345.
- Ervens, B., Sorooshian, A., Aldhaif, A.M., Shingler, T., Crosbie, E., Ziemba, L., Campuzano-Jost, P., Jimenez, J.L., Wisthaler, A., 2018. Is there an aerosol signature of chemical cloud processing? *Atmos. Chem. Phys.* 18, 16099–16119. <https://doi.org/10.5194/acp-18-16099-2018>.
- Fahey, K.M., Pandis, S.N., 2001. Optimizing model performance: variable size resolution in cloud chemistry modeling. *Atmos. Environ.* 35, 4471–4478. [https://doi.org/10.1016/S1352-2310\(01\)00224-2](https://doi.org/10.1016/S1352-2310(01)00224-2).
- Fan, M.Y., Zhang, Y.L., Lin, Y.C., Cao, F., Zhao, Z.Y., Sun, Y., Qiu, Y.M., Fu, P.Q., Wang, Y.X., 2020a. Changes of emission sources to nitrate aerosols in Beijing after the clean air actions: evidence from dual isotope compositions. *J. Geophys. Res. Atmos.* 125, e2019JD031998. <https://doi.org/10.1029/2019JD031998>.
- Fan, M.Y., Zhang, Y.L., Lin, Y.C., Li, J., Cheng, H., An, N., Su, Y.L., Qiu, Y.M., Cao, F., Fu, P.Q., 2020. Roles of sulfur oxidation pathways in the variability in stable sulfur isotopic composition of sulfate aerosols at an urban site in Beijing, China. *Environ. Sci. Technol. Lett.* 7 (12), 883–888.
- Feng, T., Bei, N.F., Zhao, S.Y., Wu, J.R., Li, X., Zhang, T., Cao, J.J., Zhou, W.J., Li, G.H., 2018. Wintertime nitrate formation during haze days in the guanzhong basin, China: a case study. *Environ. Pollut.* 243, 1057–1067.
- Fountoukis, C., Nenes, A., 2007. ISORROPIA II: a computationally efficient thermodynamic equilibrium model for K–Ca–Mg–Na–Cl–H₂O aerosols. *Atmos. Chem. Phys.* 7, 4639–4659.
- Fu, X., Wang, S.X., Chang, X., Cai, S.Y., Xing, J., Hao, J.J., 2016. Modeling analysis of secondary inorganic aerosols over China: pollution characteristics, and meteorological and dust impacts. *Sci. Rep.-UK* 6 (1), 35992.
- Gao, M., Carmichael, G.R., Wang, Y.S., Ji, D.S., Liu, Z.R., Wang, Z.F., 2016. Improving simulations of sulfate aerosols during winter haze over northern China: the impacts of heterogeneous oxidation by NO₂. *Front. Environ. Sci. Eng.* 10 (5).
- Gao, M., Han, Z.W., Liu, Z.R., Li, M., Xin, J.Y., Tao, Z.N., Li, J.W., Kang, J.E., Huang, K., Dong, X.Y., Zhuang, B.L., Li, S., Ge, B.Z., Wu, Q.Z., Cheng, Y.F., Wang, Y.S., Lee, H.J., Kim, C.H., Fu, J.S., Wang, T.J., Chin, M., Woo, J.H., 2018. Air quality and climate change, topic 3 of the model inter-comparison study for Asia phase III (MICS-Asia III) – part 1: overview and model evaluation. *Atmos. Chem. Phys.* 18, 4859–4884. <https://doi.org/10.5194/acp-18-4859-2018>.
- Grell, G.A., Dezso, D., 2002. A generalized approach to parameterizing convection combining ensemble and data assimilation techniques. *Geophys. Res. Lett.* 29, 1693.
- Grell, G.A., Peckham, S.E., Schmitz, R., Mckeen, S.A., Frost, G., Skamarock, W.C., Eder, B., 2005. Fully coupled “online” chemistry within the WRF model. *Atmos. Environ.* 39 (37), 6957–6975.
- Gultepe, I., Müller, M.D., Boybeyi, Z., 2006. A new visibility parameterization for warm-fog applications in numerical weather prediction models. *J. Appl. Meteorol. Climatol.* 45, 1469–1480. <https://doi.org/10.1175/JAM2423.1>.
- Guo, H., Weber, R.J., Nenes, A., 2017. High levels of ammonia do not raise fine particle pH sufficiently to yield nitrogen oxide-dominated sulfate production. *Sci. Rep.-UK* 7, 12109. <https://doi.org/10.1038/s41598-017-11704-0>.
- Harris, E., Sinha, B., van Pinxteren, D., Tilgner, A., Fomba, K.W., Schneider, J., Roth, A., Gnauk, T., Fahlbusch, B., Mertes, S., Lee, T., Collett, J., Foley, S., Borrmann, S., Hoppe, P., Herrmann, H., 2013. Enhanced role of transition metal ion catalysis during in-cloud oxidation of SO₂. *Science* 340, 727–730.
- Hong, L., Zhu, B., Yu, X.N., Shi, S.S., Che, K., Xia, L., 2019. Chemical composition of dew water at a suburban site in Nanjing, China, during the 2016–2017 winter. *Atmos. Environ.* 211, 226–233.
- Hong, S.Y., Noh, Y., Dudhia, J., 2006. A new vertical diffusion package with an explicit treatment of entrainment processes. *Mon. Weather Rev.* 134 (9), 2318.
- Huang, L., An, J., Koo, B., Yarwood, G., Yan, R., Wang, Y., Huang, C., Li, L., 2019. Sulfate formation during heavy winter haze events and the potential contribution from heterogeneous SO₂ + NO₂ reactions in the Yangtze River Delta region, China. *Atmos. Chem. Phys.* 19, 14311–14328. <https://doi.org/10.5194/acp-19-14311-2019>.
- Huang, R.J., Zhang, Y., Bozzetti, C., Ho, K.F., Cao, J.J., Han, Y., Daellenbach, K.R., Slowik, J.G., Platt, S.M., Canonaco, F., Zotter, P., Wolf, R., Pieber, S.M., Bruns, E.A., Crippa, M., Ciarelli, G., Piazzalunga, A., Schwikowski, M., Abbaszade, G., Schnellkreis, J., Zimmermann, R., An, Z., Szidat, S., Baltensperger, U., Haddad, I.E., Prevot, A.S.H., 2014. High secondary aerosol contribution to particulate pollution during haze events in China. *Nature* 514, 218–222. <https://doi.org/10.1038/nature13774>.
- Hung, H.M., Hoffmann, M.R., 2015. Oxidation of gas-phase SO₂ on the surfaces of acidic microdroplets: implications for sulfate and sulfate radical anion formation in the atmospheric liquid phase. *Environ. Sci. Technol.* 49 (23), 13768–13776.
- Hung, H.M., Hsu, M.N., Hoffmann, M.R., 2018. Quantification of SO₂ oxidation on interfacial surfaces of acidic micro-droplets: implication for ambient sulfate formation. *Environ. Sci. Technol.* 52 (16), 9079–9086.
- Jacob, D.J., 2000. Heterogeneous chemistry and tropospheric ozone. *Atmos. Environ.* 34, 2131–2159.
- Jia, X.C., Quan, J.N., Zheng, Z.Y., Liu, X.G., Liu, Q., He, H., Liu, Y.G., 2019. Impacts of anthropogenic aerosols on fog in North China plain. *J. Geophys. Res. Atmos.* 124, 252–265. <https://doi.org/10.1029/2018JD029437>.
- Kay, J.E., Hillman, B.R., Klein, S.A., Zhang, Y., Medeiros, B., Pincus, R., Gettelman, A., Eaton, B., Boyle, J., Marchand, R., Ackerman, T.P., 2012. Exposing global cloud biases in the community atmosphere model (CAM) using satellite observations and their corresponding instrument simulators. *J. Clim.* 25 (15), 5190–5207. <https://doi.org/10.1175/jcli-d-11-00469.1>.
- Khain, A., Leung, L.R., Lynn, B., Ghan, S., 2009. Effects of aerosols on the dynamics and microphysics of squall lines simulated by spectral bin and bulk parameterization schemes. *J. Geophys. Res. Atmos.* 114, D22203. <https://doi.org/10.1029/2009JD011902>.
- Khanal, S., Wang, Z., 2018. Uncertainties in MODIS-based cloud liquid water path retrievals at high latitudes due to mixed-phase clouds and cloud top height inhomogeneity. *J. Geophys. Res. Atmos.* 123, 11154–11172. <https://doi.org/10.1029/2018JD028558>.
- Koch, D., Park, J., Del Genio, A., 2003. Clouds and sulfate are anticorrelated: a new diagnostic for global sulfur models. *J. Geophys. Res.* 108 (D24), 4781. <https://doi.org/10.1029/2003JD003621>.
- Kong, L.D., Yang, Y.W., Zhang, S.Q., Zhao, X., Du, H.H., Fu, H.B., Zhang, S.C., Cheng, T.T., Yang, X., Chen, J.M., Wu, D., Shen, J.D., Hong, S.M., Jiao, L., 2014. Observations of linear dependence between sulfate and nitrate in atmospheric particles. *J. Geophys. Res. Atmos.* 119 (1), 341–361.
- Li, G.H., Bei, N.F., Cao, J.J., Hu, R.J., Wang, J.R., Feng, T., Wang, Y.C., Liu, S.X., Zhang, Q., Tie, X.X., Molina, L.T., 2017a. A possible pathway for rapid growth of sulfate during haze days in China. *Atmos. Chem. Phys.* 17, 3301–3316.
- Li, J., Chen, X.S., Wang, Z.F., Du, H.Y., Wang, Y.W., Sun, Y.L., Hu, B., Li, J.J., Wang, W., Wang, T., Fu, P.Q., Huang, H.L., 2018. Radiative and heterogeneous chemical effects of aerosols on ozone and inorganic aerosols over East Asia. *Sci. Total Environ.* 622–623, 1327–1342.
- Li, M., Zhang, Q., Kurokawa, J.-I., Woo, J.-H., He, K.B., Lu, Z.F., Ohara, T., Song, Y., Streets, D.G., Carmichael, G.R., Cheng, Y.F., Hong, C.P., Huo, H., Jiang, X.J., Kang, S., Liu, F., Su, H., Zheng, B., 2017b. MIX: a mosaic asian anthropogenic emission inventory under the international collaboration framework of the MICS-Asia and HTAP. *Atmos. Chem. Phys.* 17, 935–963.
- Li, Y., Zhang, G.Z., Pu, M.J., Zhu, P., Li, Z.H., 2008. The chemical composition of fog water in the winter of 2006 of Nanjing. (2008) *Sci. China Earth Sci.* 28 (5), 395–400 (in Chinese).
- Li, Z.Q., Guo, J.P., Ding, A.J., Liao, H., Liu, J.J., Sun, Y.L., Wang, T.J., Xue, H.W., Zhang, H.S., Zhu, B., 2017c. Aerosol and boundary-layer interactions and impact on air quality. *Natl. Sci. Rev.* 4, 810–833. <https://doi.org/10.1093/nsr/nwx117>.
- Liu, P.F., Ye, C., Xue, C.Y., Zhang, C.L., Mu, Y.J., Sun, X., 2020a. Formation mechanisms of atmospheric nitrate and sulfate during the winter haze pollution periods in Beijing: gas-phase, heterogeneous and aqueous-phase chemistry. *Atmos. Chem. Phys.* 20, 4153–4165. <https://doi.org/10.5194/acp-20-4153-2020>.
- Liu, T., Clegg, S.L., Abbatt, J.P.D., 2020b. Fast oxidation of sulfur dioxide by hydrogen peroxide in deliquesced aerosol particles. *Proc. Natl. Acad. Sci. U. S. A.* 117, 1354–1359.
- Liu, W.J., Han, Y.X., Li, J.X., Tian, X.R., Liu, Y.G., 2018. Factors affecting relative humidity and its relationship with the long-term variation of fog-haze events in the Yangtze River Delta. *Atmos. Environ.* 193, 242e250. <https://doi.org/10.1016/j.atmosenv.2018.0>.
- Liu, Y.H., Lu, K.D., Li, X., Dong, H.B., Tan, Z.F., Wang, H.C., Zou, Q., Wu, Y.S., Zeng, L.M., Hu, M., Min, K.-E., Kecorius, A., Wiedensohler, A., Zhang, Y.H., 2019. A comprehensive

- model test of the HONO sources constrained to field measurements at rural North China plain. *environ. Sci. Technol.* 53, 3517–3525.
- Lowe, D., Archer-Nicholls, S., Morgan, W., Allan, J., Utembe, S., Ouyang, B., Aruffo, E., Le Breton, M., Zaveri, R.A., Di Carlo, P., Percival, C., Coe, H., Jones, R., McFiggans, G., 2015. WRF-chem model predictions of the regional impacts of N2O5 heterogeneous processes on night-time chemistry over North-Western Europe. *Atmos. Chem. Phys.* 15 (1385–1409), 2015. <https://doi.org/10.5194/acp-15-1385-404>.
- Lu, C.S., Niu, S.J., Tang, L.L., Lv, J.J., Zhao, L.J., Zhu, B., 2010. Chemical composition of fog water in Nanjing area of China and its related fog microphysics. *Atmos. Res.* 97, 47–69.
- Luo, G., Yu, F., Schwab, J., 2019. Revised treatment of wet scavenging processes dramatically improves GEOS-chem 12.0.0 simulations of surface nitric acid, nitrate, and ammonium over the United States. *Geosci. Model Dev.* 12, 3439–3447. <https://doi.org/10.5194/gmd-12-3439-2019>.
- Ma, X.Y., Sha, T., Wang, J.Y., Jia, H.L., Tian, R., 2018. Investigating impact of emission inventories on PM2.5 simulations over North China plain by WRF-chem. *Atmos. Environ.* 195, 125–140.
- Ma, X.Y., Salzen, K.V., 2006. Dynamics of the sulphate aerosol size distribution on a global scale. *J. Geophys. Res. Atmos.* 111 (D8).
- McDuffie, E.E., Fibiger, D.L., Dube, W.P., Lopez-Hilfiker, F., Lee, B.H., Thornton, J.A., Shah, V., Jaegle, L., Guo, H., Weber, R.J., Reeves, J.M., Weinheimer, A.J., Schroder, J.C., Campuzano-Jost, P., Jimenez, J.L., Dibb, J.E., Veres, P., Ebben, C., Sparks, T.R., Wooldridge, P.J., Cohen, R.C., Hornbrook, R.S., Apel, E.C., Campos, T., Hall, S.L., Ullmann, K., Brown, S.S., 2018. Heterogeneous N2O5 uptake during Winter: aircraft measurements during the 2015 WINTER campaign and critical evaluation of current parameterizations. *J. Geophys. Res. Atmos.* 123, 4345–4372. <https://doi.org/10.1002/2018JD028336>.
- Miao, R., Chen, Q., Zheng, Y., Cheng, X., Sun, Y., Palmer, P.I., Shrivastava, M., Guo, J., Zhang, Q., Liu, Y., Tan, Z., Ma, X., Chen, S., Zeng, L., Lu, K., Zhang, Y., 2020. Model bias in simulating major chemical components of PM2.5 in China. *Atmos. Chem. Phys.* 20, 12265–12284. <https://doi.org/10.5194/acp-20-12265-2020>.
- Min, Q., Joseph, E., Lin, Y., Min, L., Yin, B., Daum, P.H., Kleinman, L.L., Wang, J., Lee, Y.-N., 2012. Comparison of MODIS cloud microphysical properties with in-situ measurements over the Southeast Pacific. *Atmos. Chem. Phys.* 12, 11261–11273. <https://doi.org/10.5194/acp-12-11261-2012>.
- Mlawer, E.J., Taubman, S.J., Brown, P.D., Iacono, M.J., Clough, S.A., 1997. Radiative transfer for inhomogeneous atmospheres: RRTM, a validated correlated-k model for the longwave. *J. Geophys. Res.* 102, 16663–16682. <https://doi.org/10.1029/97JD00237>.
- Moch, J.M., Dovrou, E., Mickley, L.J., Keutsch, F.N., Cheng, Y., Jacob, D.J., Jiang, J.K., Li, M., Munger, J.W., Qiao, X.H., Zhang, Q., 2018. Contribution of hydroxymethane sulfonate to ambient particulate matter: a potential explanation for high particulate sulfur during severe winter haze in Beijing. *Geophys. Res. Lett.* 45, 11969–11979. <https://doi.org/10.1029/2018GL079309>.
- Moch, J.M., Dovrou, E., Mickley, L.J., Keutsch, F.N., Liu, Z., Wang, Y., Dombek, T.L., Kuwata, M., Budisulistiorini, S.H., Yang, L., Decesari, S., Pagliano, M., Alexander, B., Shao, J., Munger, J.W., Jacob, D.J., 2020. Global importance of hydroxymethanesulfonate in ambient particulate matter: implications for air quality. *J. Geophys. Res.* 125, e2020JD032706.
- Mueller, S.F., Bailey, E.M., Cook, T.M., Mao, Q., 2006. Treatment of clouds and the associated response of atmospheric sulfur in the community multiscale air quality (CMAQ) modeling system. *Atmos. Environ.* 40 (35), 6804–6820. <https://doi.org/10.1016/j.atmosenv.2006.05.069>.
- Platnick, S., King, M.D., Meyer, K.G., Wind, G., Amarasinghe, N., Marchant, B., 2014. MODIS Cloud Optical Properties: User Guide for the Collection 6 Level-2 MOD06/MYD06 Product and Associated Level-3 Datasets. NASA, Greenbelt.
- Pye, H.O.T., Nenes, A., Alexander, B., Ault, A.P., Barth, M.C., Clegg, S.L., Collett Jr., J.L., Fahey, K.M., Hennigan, C.J., Herrmann, H., Kanakidou, M., Kelly, J.T., Ku, L.-T., McNeill, V.F., Riemer, N., Schaefer, T., Shi, G.L., Tilgner, A., Walker, J.T., Wang, T., Weber, R., Xing, J., Zaveri, R.A., Zundel, A., 2020. The acidity of atmospheric particles and clouds. *Atmos. Chem. Phys.* 20, 4809–4888. <https://doi.org/10.5194/acp-20-4809-2020>.
- Qin, Y.S., Liu, D.Y., Yin, Y.Y., Li, L., 2011. Analysis of chemical characteristics in fog water and pollutant source in Nanjing. *Environ. Chem.* 30 (4), 816–824.
- Qu, Z., Henze, D.K., Theys, N., Wang, J., Wang, W., 2019. Hybrid mass Balance/4D-var joint inversion of NOx and SO2 emissions in East Asia. *J. Geophys. Res. Atmos.* 124, 8203–8224. <https://doi.org/10.1029/2018JD030240>.
- Rasch, P.J., Barth, M.C., Kiehl, J.T., Schwartz, S.E., Benkovitz, C.M., 2000. A description of the global sulfur cycle and its controlling processes in the national center for atmospheric research community climate model, version 3. *J. Geophys. Res. Atmos.* 105 (D1), 1367.
- Richards, J.A., 2013. Remote Sensing Digital Image Analysis. Springer, New York, NY, USA. <https://doi.org/10.1007/978-3-642-30062-2>.
- Sarwar, G., Simon, H., Xing, J., Mathur, R., 2014. Importance of tropospheric ClNO2 chemistry across the northern hemisphere. *Geophys. Res. Lett.* 41, 4050–4058. <https://doi.org/10.1002/2014GL059962>.
- Sarwar, G., Simon, H., Bhawe, P., Yarwood, G., 2012. Examining the impact of heterogeneous nitril chloride production on air quality across the United States. *Atmos. Chem. Phys.* 12, 6455–6473. <https://doi.org/10.5194/acp-12-6455-2012>. www.atmos-chem-phys.net/12/6455/2012/.
- Sha, T., Ma, X.Y., Jia, H.L., Tian, R., Chang, Y.H., Cao, F., Zhang, Y.L., 2019a. Aerosol chemical component: simulations with WRF-Chem and comparison with observations in Nanjing. *Atmos. Environ.* 218, 116982. <https://doi.org/10.1016/j.atmosenv.2019.116982>.
- Sha, T., Ma, X.Y., Jia, H.L., van der A, R.J., Ding, J.Y., Zhang, Y.L., Chang, Y.H., 2019b. Exploring the influence of two inventories on simulated air pollutants during winter over the Yangtze River Delta. *Atmos. Environ.* 206, 170–182.
- Shah, V., Jacob, D.J., Moch, J.M., Wang, X., Zhai, S., 2020. Global modeling of cloud water acidity, precipitation acidity, and acid inputs to ecosystems. *Atmos. Chem. Phys.* 20, 12223–12245. <https://doi.org/10.5194/acp-20-12223-2020>.
- Shao, J.Y., Chen, Q.J., Wang, Y.X., Lu, X., He, P.Z., Sun, Y.L., Shah, V., Martin, R.V., Philip, S., Song, S.J., Zhao, Y., Xie, Z.Q., Zhang, L., Alexander, B., 2019. Heterogeneous sulfate aerosol formation mechanisms during wintertime Chinese haze events: air quality model assessment using observations of sulfate oxygen isotopes in Beijing. *Atmos. Chem. Phys.* 19, 6107–6123.
- Song, S., Gao, M., Xu, W., Sun, Y., Worsnop, D.R., Jayne, J.T., Zhang, Y., Zhu, L., Li, M., Zhou, Z., Cheng, C., Lv, Y., Wang, Y., Peng, W., Xu, X., Lin, N., Wang, Y., Wang, S., Munger, J.W., Jacob, D.J., McElroy, M.B., 2019. Possible heterogeneous chemistry of hydroxymethanesulfonate (HMS) in northern China winter haze. *Atmos. Chem. Phys.* 19, 1357–1371. <https://doi.org/10.5194/acp-19-1357-2019>.
- Sorooshian, A., Brechtel, F.J., Ervens, B., Feingold, G., Varutbangkul, V., Bahreini, R., Murphy, S., Holloway, J.S., Atlas, E.L., Anlauf, K., Buzorius, G., Jonsson, H., Flagan, R.C., Seinfeld, J.H., 2006. Oxalic acid in clear and cloudy atmospheres: analysis of data from International Consortium for Atmospheric Research on Transport and Transformation 2004. *J. Geophys. Res. Atmos.* 111, D23545. <https://doi.org/10.1029/2005JD006880>.
- Sorooshian, A., Lu, M.-L., Brechtel, F.J., Jonsson, H., Feingold, G., Flagan, R.C., Seinfeld, J.H., 2007. On the source of organic acid aerosol layers above clouds. *Environ. Sci. Technol.* 41, 4647–4654.
- Su, T., Li, Z., Kahn, R., 2018. Relationships between the planetary boundary layer height and surface pollutants derived from lidar observations over China: regional pattern and influencing factors. *Atmos. Chem. Phys.* 18, 15921–15935. <https://doi.org/10.5194/acp-18-15921-2018>.
- Sukoriansky, S., Galperin, B., Perov, V., 2005. Application of a new spectral model of stratified turbulence to the atmospheric boundary layer over sea ice. *Bound. Layer Meteorol.* 117, 231–257. <https://doi.org/10.1007/s10546-004-6848-4>.
- Tewari, M., Chen, F., Wang, W., Dudhia, J., LeMone, M.A., Mitchell, K., Ek, M., Gayno, Wegiel, G.J., Cuenca, R.H., 2004. Implementation and verification of the unified NOAA land surface model in the WRF model (Formerly Paper Number 17.5). 20th Conference on Weather Analysis and Forecasting/16th Conference on Numerical Weather Prediction, pp. 11–15.
- Tian, R., Ma, X., Sha, T., Pan, X., Wang, Z., 2021. Exploring dust heterogeneous chemistry over China: insights from field observation and GEOS-chem simulation. *Sci. Total Environ.* 798 (12), 149307.
- Wang, G.H., Zhang, R.Y., Gomez, M.E., Yang, L.X., Zamora, M.L., Hu, M., Lin, Y., Peng, J.F., Guo, S., Meng, J.J., Li, J.J., Cheng, C.L., Hu, T.F., Ren, Y.Q., Wang, X.S., Gao, J., An, Z.S., Zhou, W.J., Li, G.H., Wang, J.Y., Tian, Y.Q., Marrero-Ortiz, W., Secret, J., Du, Z.F., Zheng, J., Dongjie, S., Zeng, L., Shao, M., Wang, W.G., Huang, Y., Wang, Y., Zhu, Y.J., Li, Y.X., Hu, J.X., Pan, B., Cai, L., Cheng, Y.T., Ji, Y.M., Zhang, F., Rosenfeld, D., Liss, P.S., Duce, R.A., Kolb, C.E., Molina, M.J., 2016a. Persistent sulfate formation from London fog to Chinese haze. *Proc. Natl. Acad. Sci. U. S. A.* 113, 13630–13635.
- Wang, J.F., Li, J.Y., Ye, J.H., Zhao, J., Wu, Y.Z., Hu, J.L., Liu, D.T., Nie, D.Y., Shen, F.Z., Huang, X.P., Huang, D.D., Ji, D.S., Sun, X., Xu, W.Q., Guo, J.P., Song, S.J., Qin, Y.M., Liu, P.F., Turner, J.R., Lee, H.C., Hwang, S., Liao, H., Martin, S.T., Zhang, Q., Chen, M.O.D., Sun, Y.L., Ge, X.L., Jacob, D.J., 2020. Fast sulfate formation from oxidation of SO2 by NO2 and HONO observed in Beijing haze. *Nat. Commun.* 11, 2844. <https://doi.org/10.1038/s41467-020-16683-x>.
- Wang, J., Park, S., Zeng, J., Ge, C., Yang, K., Carn, S., Krotkov, N., Omar, A.H., 2013a. Modeling of 2008 kasatochi volcanic sulfate direct radiative forcing: assimilation of OMI SO2 plume height data and comparison with MODIS and CALIOP observations. *Atmos. Chem. Phys.* 13, 1895–1912. <https://doi.org/10.5194/acp-13-1895-2013>.
- Wang, Y.C., Chen, J., Wang, Q.Y., Qin, Q.D., Ye, J.H., Han, Y.M., Li, L., Zhen, W., Zhi, Q., Zhang, Y.X., Cao, J.J., 2019. Increased secondary aerosol contribution and possible processing on polluted winter days in China. *Environ. Int.* 127, 78–84. <https://doi.org/10.1016/j.envint.2019.03.021>.
- Wang, Y.S., Yao, L., Wang, L.L., Liu, Z.R., Ji, D.S., Tang, G.Q., Zhang, J.K., Sun, Y.L., Hu, B., Xin, J.Y., 2013b. Mechanism for the formation of the January 2013 heavy haze pollution episode over central and eastern China. *Sci. China Earth Sci.* 57, 14–25. <https://doi.org/10.1007/s11430-013-4773-4>.
- Wang, Y.X., Zhang, Q.Q., Jiang, J.K., Zhou, W., Wang, B.Y., He, K.B., Duan, F.K., Zhang, Q., Philip, S., Xie, Y.Y., 2014. Enhanced sulfate formation during China's severe winter haze episode in January 2013 missing from current models. *J. Geophys. Res. Atmos.* 119 (11), 10425–10440. <https://doi.org/10.1002/2013JD021426>.
- Wang, Y., Wang, J., Xu, X., Henze, D.K., Wang, Y., Qu, Z., 2016b. A new approach for monthly updates of anthropogenic sulfur dioxide emissions from space: application to China and implications for air quality forecasts. *Geophys. Res. Lett.* 43, 9931–9938. <https://doi.org/10.1002/2016GL070204>.
- Weber, R.J., Guo, H., Russell, A.G., Nenes, A., 2016. High aerosol acidity despite declining atmospheric sulfate concentrations over the past 15 years. *Nat. Geosci.* 9, 282–285. <https://doi.org/10.1038/ngeo2665>.
- Wonaschuetz, A., Sorooshian, A., Ervens, B., Chuang, P.Y., Feingold, G., Murphy, S.M., de Gouw, J., Warneke, C., Jonsson, H.H., 2012. Aerosol and gas re-distribution by shallow cumulus clouds: an investigation using airborne measurements. *J. Geophys. Res. Atmos.* 117, D17202. <https://doi.org/10.1029/2012JD018089>.
- Wu, J.R., Bei, N.F., Hu, B., Liu, S.X., Zhou, M., Wang, Q.Y., Li, X., Liu, L., Feng, T., Liu, Z.R., Wang, Y.C., Cao, J.J., Tie, X.X., Wang, J., Molina, L.T., Li, G.H., 2019. Is water vapor a key player of the wintertime haze in North China Plain? *Atmos. Chem. Phys.* 19, 8721–8739. <https://doi.org/10.5194/acp-19-8721-2019>.
- Xie, Y.Y., Wang, Y.X., Dong, W.H., Wright, J.S., Shen, L., Zhao, Z.J., 2019. Evaluating the response of summertime surface sulfate to hydroclimate variations in the continental United States: role of meteorological inputs in the GEOS-chem model. *J. Geophys. Res. Atmos.* 124. <https://doi.org/10.1029/2018JD029693>.

- Xu, L.L., Duan, F.K., He, K.B., Ma, Y.L., Zhu, L.D., Zheng, Y.X., Huang, T., Kimoto, T., Ma, T., Li, H., Ye, S., Yang, S., Sun, Z.L., Xu, B.Y., 2017. Characteristics of the secondary water-soluble ions in a typical autumn haze in Beijing. *Environ. Pollut.* 227, 296–305. <https://doi.org/10.1016/j.envpol.2017.04.076>.
- Xue, J., Yuan, Z.B., Griffith, S.M., Yu, X., Lau Alexis, K.H., Yu, J.Z., 2016. Sulfate formation enhanced by a cocktail of high NO_x, SO₂, particulate matter, and droplet pH during haze-fog events in megacities in China: an observation-based modeling investigation. *Environ. Sci. Technol.* 50, 7325–7334. <https://doi.org/10.1021/acs.est.6b00768>.
- Yan, S., Zhu, B., Huang, Y., Zhu, J., Kang, H., Lu, C., Zhu, T., 2020. To what extents do urbanization and air pollution affect fog? *Atmos. Chem. Phys.* 20, 5559–5572. <https://doi.org/10.5194/acp-20-5559-2020>.
- Yan, W.L., Zhang, G.Z., Pu, M.J., Liu, D.Y., Li, Z.H., 2013. Chemical features and cause analysis of a strong acid fog event in Nanjing. *J. Nat. Dis.* 22 (3), 122–129 (in Chinese).
- Yang, J., Xie, Y.J., Shi, C.E., Liu, D.Y., Niu, S.J., Li, Z.H., 2009. Difference in ion composition of winter fog water between radiation and advection-radiation fog episodes in Nanjing. *Trans. Atmos. Sci.* 32 (6), 776–782.
- Ye, C., Liu, P., Ma, Z., Xue, C., Zhang, C., Zhang, Y., Liu, J.F., Liu, C.T., Sun, X., Mu, Y.J., 2018. High H₂O₂ concentrations observed during haze periods during the winter in Beijing: importance of H₂O₂ oxidation in sulfate formation. *Environ. Sci. Technol. Lett.* 5 (12), 757–763.
- Zaveri, R.A., Peters, L.K., 1999. A new lumped structure photochemical mechanism for large-scale applications. *J. Geophys. Res. Atmos.* 104, 30387–30415.
- Zaveri, R.A., Easter, R.C., Fast, J.D., Peters, L.K., 2008. Model for simulating aerosol interactions and chemistry (MOSAIC). *J. Geophys. Res. Atmos.* 113, D13204.
- Zhan, Y., Xie, M., Gao, D., Wang, T., Zhang, M., An, F., 2021. Characterization and source analysis of water-soluble inorganic ionic species in PM_{2.5} during a wintertime particle pollution episode in Nanjing, China. *Atmos. Res.* 105769.
- Zhang, L., Chen, Y.F., Zhao, Y.H., Henze, D.K., Zhu, L.Y., Song, Y., Paulot, F., Liu, X.J., Pan, Y.P., Lin, Y., Huang, B.X., 2018. Agricultural ammonia emissions in China: reconciling bottom-up and top-down estimates. *Atmos. Chem. Phys.* 18, 339–355. <https://doi.org/10.5194/acp-18-339-2018>.
- Zheng, B., Zhang, Q., Zhang, Y., He, K.B., Wang, K., Zheng, G.J., Duan, F.K., Ma, Y.L., Kimoto, T., 2015a. Heterogeneous chemistry: a mechanism missing in current models to explain secondary inorganic aerosol formation during the January 2013 haze episode in North China. *Atmos. Chem. Phys.* 15, 2031–2049.
- Zheng, G.J., Duan, F.K., Su, H., Ma, Y.L., Cheng, Y., Zheng, B., Zhang, Q., Huang, T., Kimoto, T., Chang, D., Poschl, U., Cheng, Y.F., He, K.B., 2015b. Exploring the severe winter haze in Beijing: the impact of synoptic weather, regional transport and heterogeneous reactions. *Atmos. Chem. Phys.* 15, 2969–2983. <https://doi.org/10.5194/acp-15-2969-2015>.
- Zhou, B., Du, J., 2010. Fog prediction from a multimodel mesoscale ensemble prediction system. *Weather Forecast.* 25 (1), 303–322. <https://doi.org/10.1175/2009WAF2222289.1>.
- Zhu, D.D., Fan, S.X., Hu, C.Y., Zhang, H.W., Zhang, S.R., Zhang, L.Y., 2020. Characteristics of organic acids and inorganic components in three-stage fog water in Nanjing. (2020) *China Environ. Sci.* 40 (8), 3342–3351 (in Chinese).
- Zou, J., Sun, J., Li, T., Han, X., Xiang, Z., Sha, J., 2020. Observed interactions among haze, fog and atmospheric boundary layer during a haze-fog episode in the Yangtze River Delta Region, Eastern China. *Aerosol Air Qual. Res.* <https://doi.org/10.4209/aaqr.2020.06.0354>.